

1 **Scaling Potential Evapotranspiration with Greenhouse Warming**

2 JACOB SCHEFF * AND DARGAN M. W. FRIERSON

Atmospheric Sciences, University of Washington, Seattle, WA

* *Corresponding author address:* Jacob Scheff, Dept. of Atmospheric Sciences, Box 351640, Seattle, WA 98195-1640.

E-mail: jscheff@uw.edu

ABSTRACT

Potential evapotranspiration (PET) is a supply-independent measure of the evaporative demand of a terrestrial climate, of basic importance in climatology, hydrology, and agriculture. Future increases in PET from greenhouse warming are often cited as key drivers of global trends toward drought and aridity. The present work computes recent and business-as-usual future Penman-Monteith PET fields at 3-hourly resolution in 13 modern global climate models. The %-change in local annual-mean PET over the upcoming century is almost always positive, modally low double-digit in magnitude, usually increasing with latitude, yet quite divergent between models.

These patterns are understood as follows. In every model, the global field of PET %-change is found to be dominated by the direct, positive effects of constant-relative-humidity warming (via increasing vapor deficit and increasing Clausius-Clapeyron slope.) This direct-warming term accurately scales as the PET-weighted (warm-season daytime) local warming, times 5-6% per degree (related to the Clausius-Clapeyron equation), times an analytic factor ranging from about 0.25 in warm climates to 0.75 in cold climates, plus a small correction. With warming of several degrees, this product is of low double-digit magnitude, and the strong temperature dependence gives the latitude dependence. Similarly, the inter-model spread in the amount of warming gives most of the spread in this term. Additional spread in the total change comes from strong disagreement on radiation, relative-humidity, and windspeed changes, which make smaller yet substantial contributions to the full PET %-change fields.

24 1. Introduction

25 a. *Why potential evapotranspiration?*

26 Potential evapotranspiration (PET), a basic land climate variable (e.g. Hartmann 1994),
27 is the rate at which a given climate is trying to evaporate water from the soil-vegetation
28 system. In other words, for given atmospheric and radiative conditions, PET is the surface
29 evapotranspiration (ET) rate that would hold if the soil and vegetation were well-watered.
30 Synonymous and near-synonymous concepts include reference evapotranspiration, potential
31 evaporation, evaporative demand, and pan evaporation. Critically, PET may be thought of
32 as the water required to maintain a garden or irrigated crop, or the water “price” a plant
33 must pay to maintain open stomata. A higher-PET climate is thus a more arid, evaporative
34 climate. Therefore, in this study we attempt to understand how local PET will scale with
35 global greenhouse warming, using global climate models (GCMs) as well as basic physical
36 principles.

37 PET is also of interest because it is a key factor explaining other hydrologic and climatic
38 quantities. Several prominent conceptual models of land hydrology, including the Palmer
39 Drought Severity Index (PDSI; Palmer 1965) and the Budyko and Miller (1974) ecohydro-
40 logic theory, take precipitation (water supply) and PET (water demand) as climate-supplied
41 forcings, and give soil moisture, actual ET (latent heat) flux, runoff, and/or drought index
42 as land-generated responses. In these sorts of frameworks, understanding precipitation and
43 PET changes are necessary for understanding other land hydroclimatic changes. In par-
44 ticular, recent studies using the PDSI to warn of widespread drought increases with future
45 greenhouse warming (e.g. Dai 2013; Burke et al. 2006) cite systematic global PET increases
46 as the main driver of their alarming results. Understanding the nature, magnitude and
47 pattern of these projected increases is the motive of the present work.

48 Additionally, PET is a more natural choice than actual ET for the evaporative component
49 of land “aridity” metrics because changes in actual ET often just reflect supply (precipita-

tion) changes. For example, the well-known study of Seager et al. (2007) uses precipitation minus actual ET ($P - E$) to quantify modeled aridification due to greenhouse warming in a subtropical, terrestrial region where the model precipitation declines a great deal. The model ET (Seager et al.'s E) in this area also significantly declines, not surprisingly. However, the analysis, by its nature, interprets the ET decline as if it is some other factor helping to offset or mitigate the precipitation decline. In fact, the model climate is probably becoming more evaporative, not less, due to warming and (presumably) cloud-cover and relative-humidity reduction, and this should not mitigate but aggravate the local ecological effect of the precipitation reduction, even though the actual evaporative flux necessarily decreases due to the supply decrease (e.g. Brutsaert and Parlange 1998). To avoid this type of pitfall, the aridity of a climate is usually quantified using the ratio P/PET of annual water supply to annual water demand, or similar (e.g. Budyko and Miller 1974; Middleton and Thomas 1997; Mortimore 2009), which has the additional advantage of being dimensionless. $P/PET < 0.05$ is then defined as hyperarid, $0.05 < P/PET < 0.2$ as arid, $0.2 < P/PET < 0.5$ as semiarid, and so forth. Feng and Fu (2013) show that global climate models project systematic future decreases in P/PET (i.e. aridification) over most of Earth's land, again owing to the (projected) systematic PET increases that we attempt to understand in this work.

b. Quantifying PET

Except where an evaporation pan, lysimeter or other direct method is available, PET cannot be measured in the field, so it is usually estimated from its meteorological and/or radiative causes. Several estimation methods are in wide use. All of the above studies of greenhouse-driven future drought or aridity expansion (Dai 2013; Burke et al. 2006; Feng and Fu 2013) use the Penman-Monteith equation, a fundamental physics-based method (Penman 1948; Monteith 1981). Given some near-surface air temperature T_a , water-vapor pressure e_a , windspeed $|u|$, and net downward broadband radiation R_n , this equation simply gives the latent heat flux LH (equivalent to ET) that solves the system

$$\text{SH} = \frac{\rho_a c_p (T_s - T_a)}{r_a} \quad (1)$$

$$\text{LH} = \frac{\rho_a c_p (e^*(T_s) - e_a)}{\gamma (r_s + r_a)} \quad (2)$$

$$R_n - G = \text{SH} + \text{LH} \quad (3)$$

76 for the three unknowns SH (sensible heat flux), LH, and T_s (skin temperature that would
 77 hold under well-watered conditions.) Here, (1) is the bulk formula for SH, (2) is the bulk
 78 formula for LH under well-watered conditions, (3) is the surface energy budget, $e^*(T)$ is the
 79 saturation vapor pressure at a given temperature T , $r_a = 1/(C_H |u|)$ is the aerodynamic
 80 resistance between the canopy surface and the level where T_a and e_a are measured, C_H is a
 81 scalar transfer coefficient, r_s is the bulk stomatal resistance under well-watered conditions,
 82 G is the heat flux into the ground or soil (usually parameterized or ignored), ρ_a is the air
 83 density, c_p is the air specific heat, $\gamma = (c_p p_s) / (\varepsilon L_v)$ is the collection of constants from having
 84 written (2) in a manner analogous to (1), p_s is the surface air pressure, $\varepsilon \approx 0.622$ is the ratio
 85 of molar masses of water vapor and dry air, and L_v is the latent heat of vaporization of
 86 water.

87 The solution to this system proceeds by noting that if $T_s - T_a$ isn't too large, then
 88 $e^*(T_s) \approx e^*(T_a) + de^*/dT(T_a)(T_s - T_a)$, which allows T_s to be cleanly eliminated between
 89 (1) and (2), giving (with the help of (3))

$$\text{LH} = \frac{\Delta (R_n - G) + \rho_a c_p (e^*(T_a) - e_a) C_H |u|}{\Delta + \gamma (1 + r_s C_H |u|)}, \quad (4)$$

90 the surface latent heat flux that would hold under well-watered conditions with the given
 91 meteorology and radiation. Here $\Delta := de^*/dT(T_a)$ is the standard shorthand for the local
 92 slope of the Clausius-Clapeyron curve, which will be used from now on. By definition, this

93 flux (divided by L_v) is the potential evapotranspiration. The resulting formula (5) is the
 94 *Penman-Monteith equation*:

$$\text{PET} = \left(\frac{\Delta (R_n - G) + \rho_a c_p e^*(T_a) (1 - \text{RH}) C_H |u|}{\Delta + \gamma (1 + r_s C_H |u|)} \right) / L_v. \quad (5)$$

95 The first term in the numerator of (5) is known as the *radiative term*, and the second
 96 is called the *aerodynamic term*. Note that in the latter we have rewritten $e^*(T_a) - e_a$, the
 97 *vapor pressure deficit* appearing in (4), as $e^*(T_a) (1 - \text{RH})$ where RH is the near-surface
 98 relative humidity. This allows changes in the vapor pressure deficit to be separated into
 99 constant-RH changes in e^* (from T_a changes), and constant- T_a changes in RH. (From here
 100 on we are dropping the (T_a) and simply writing e^* for $e^*(T_a)$, since T_s has been eliminated.)

101 Many of the input variables in (5) will change with significant greenhouse warming. Most
 102 immediately, the surface net radiation R_n will tend to increase (absent any cloud feedbacks)
 103 because of the extra longwave emitters in the atmosphere, sending more longwave energy
 104 back at the surface. This alone would tend to increase PET (5). However, the warming
 105 itself will also directly change PET through e^* and Δ , which both increase with T_a by the
 106 Clausius-Clapeyron law. Constant-RH increases in e^* will increase PET by widening the
 107 vapor pressure deficit, especially where and when RH is low. (The discussion in the review
 108 paper of Roderick et al. (2009) omitted this mechanism.) Increases in Δ may increase or
 109 decrease PET depending on the magnitudes of various terms in (5). It is not clear a priori
 110 whether the radiation changes or these direct-warming changes will dominate.

111 In addition, RH might change in either direction, through a common theoretical expecta-
 112 tion for RH is that it should remain roughly constant (e.g. Held and Soden 2000), as
 113 generally observed thus far (e.g. Held and Soden 2006). This is the main motivation for
 114 considering constant-RH e^* changes separately from changes in RH.

115 Finally, raw observations indicate that $|u|$ decreased in most land areas over the past
 116 several decades (McVicar et al. 2012), in sufficient magnitude to overcome the concurrent T_a
 117 increases in (5) and explain the widespread observations of declining pan evaporation, i.e.

118 *declining* PET (McVicar et al. 2012; Roderick et al. 2009; Wang et al. 2012). However, it is
119 still unclear whether or not this terrestrial wind “stilling” is a measurement artifact, as it does
120 not appear in reanalyses (e.g. Pryor et al. 2009; McVicar et al. 2008) or marine observations
121 (McVicar et al. 2012), and some of the pan-evaporation declines themselves are also raw
122 and unadjusted for observing-system changes. Even if real, it is highly unclear whether the
123 stilling is due to global warming (McVicar et al. 2012), and it may have reversed course after
124 about 1998 (Wang et al. 2012). Therefore, in this study we take the future model output
125 of $|u|$ at face value, which contains no such systematic declines. However, if any real global
126 stilling trend of the proposed magnitude were to continue unabated into future decades,
127 PET would presumably continue declining and the conclusions of our study (as well as those
128 mentioned above) would not apply.

129 Other, non-Penman methods of estimating PET are also in use, as mentioned at the
130 beginning of this subsection. The Thornthwaite (1948) method and other *temperature-proxy*
131 *methods* empirically relate PET to T_a alone, for a given location and time of year. This
132 simplicity has encouraged their frequent use for variability in the current climate (e.g. Palmer
133 1965), which has led some studies to use them, or models containing them, to assess future
134 climate change (e.g. Wehner et al. 2011; Price and Rind 1994); see also references in Lofgren
135 et al. (2011). However, within a given climate (especially during warm, high-PET parts of the
136 year), anomalous warmth is associated with anomalous sunshine (higher R_n), and often also
137 with anomalous low RH, significantly enlarging the positive response of (5). By contrast,
138 future climate change should warm T_a *without* the sunshine and RH changes that might
139 accompany a similar warm anomaly in year-to-year variability. Thus one would expect from
140 (5) that an empirically determined dependence of PET on T_a from year-to-year variation
141 would overestimate the greenhouse climate change response. Indeed, several studies (e.g.
142 McKenney and Rosenberg 1993; Hobbins et al. 2008) have found that the same long-term
143 climatic changes can imply large increases in Thornthwaite PET but much smaller increases,
144 or even slight decreases in Penman-Monteith PET. Similarly, negative PDSI responses to

145 future global climate model output are 2-3 times stronger using the default Thornthwaite
146 PET than using Penman-Monteith PET (A. Dai, pers. comm.) Thus, studies that use a
147 simple temperature-proxy method to assess future PET changes may be severely flawed.

148 Other studies of future climate change (Lofgren et al. 2011; Arora 2002) simply estimate
149 PET as R_n/L_v , which we will call the *energy-only method*. While this works reasonably well
150 for spatial differences in the present climate (Budyko and Miller 1974), one would presume
151 that it *underestimates* future PET increases because it doesn't include the independent
152 physical effects of T_a through the Clausius-Clapeyron law, discussed above.

153 Still other studies of PET change in global climate models (e.g. Rind et al. 1990) have
154 directly used an internal land-model field that is also called "potential evapotranspiration."
155 However, this field is (quite confusingly) not the same concept as what we have been dis-
156 cussing: it is what would *instantaneously* start evaporating if the surface were to be suddenly
157 wettened, without any chance to cool down the skin temperature T_s and establish energy
158 balance (3) with R_n . In other words, this field is directly computed using the bulk LH
159 formula (2), where r_s is still the well-watered "open" stomatal resistance but T_s is now the
160 actual skin-temperature output of the model instead of the well-watered skin-temperature
161 used above, which is often much cooler. Indeed, Rind et al. (1990) (and references therein)
162 found that this model "PET" achieved summertime climatological values averaged over the
163 United States of $\sim 40 \text{ mm day}^{-1}$ in the climate models of their day. (The observed sum-
164 mertime PET maxima in, e.g., Hartmann (1994) are almost an order of magnitude lower.)
165 So this quantity, while interesting perhaps, is not the object of our study (and also it is not
166 publicly archived in CMIP5 by any of the models.)

167 Therefore, in this study we use (5) to quantify and understand the PET response to
168 future greenhouse warming.

2. Methods

Penman-Monteith PET (5) is usually many times larger in magnitude during the day than at night, because of both R_n and the vapor-pressure deficit. Thus, daytime climate changes may affect time-integrated PET much more than nighttime climate changes, so it is desirable to examine diurnally resolved climate and PET. In the recent fifth phase of the Coupled Model Intercomparison Project (CMIP5; Taylor et al. 2012), sub-daily surface output is conveniently accessible for the first time, at 3-hourly resolution. 16 of the CMIP5 global climate models archive all of the necessary information (surface energy budget terms and near-surface temperature, moisture, and wind) at this resolution for years 2081-99 in the business-as-usual “rcp8.5” scenario and 1981-99 in the historical scenario. However, in 3 of these, the meteorological fields are given at, say, 10 m above the soil surface, instead of 10 m above the canopy top (M. Watanabe, pers. comm.), making them inapplicable to (1) and (2) (and thus (5)) in forest areas. So, we use the remaining 13 models, which we list in Table 1 along with any model-specific exceptions to our procedures. We use output from run 1 (“r1i1p1” in CMIP5 filenames) only.

A prominent version of (5) is the recent ASCE (American Society of Civil Engineers) Standardized Reference Evapotranspiration Equation (Allen et al. 2005), which was explicitly developed for the purpose of standardizing the computation of reference or potential ET for all users. The development included the systematic intercomparison and testing of numerous operationally used Penman-type methods. Our full method closely based on Allen et al. (2005) is given in section a of the Appendix. Briefly, we fix C_H and r_s as universal constants corresponding to “alfalfa” values as specified by Allen et al. (2005), with $C_H \approx 5.7 \times 10^{-3}$, and r_s varying between 30 s m^{-1} (day) and 200 s m^{-1} (night). (We will see in section 5 that our conclusions are not very sensitive to these vegetation parameters.) We also compute $(R_n - G)$ as $LH + SH$ (3) because the models do not output G , and we let e^* , Δ and ρ_a depend on T_a as specified in Allen et al. (2005).

Using these procedures and values, for each of the 13 CMIP5 models in Table 1 we

196 compute Penman-Monteith PET (5) for every model grid cell that is at least 80% ice-
197 free land and for every 3-hour interval comprising the 19-year epochs 1981-99 and 2081-99
198 (except those that fall on 29 Feb in models which use the full gregorian calendar.) For each
199 interval in the calendar year, we average over the 19 years to obtain a diurnally and annually
200 varying PET climatology of each epoch. Averaging over the calendar then gives annual-mean
201 climatologies of PET. These are shown for 1981-99 in Figure 1 along with their multimodel
202 means, and appear quite reasonable with higher modeled PET in sunnier, lower-RH and/or
203 warmer locations. As an additional reality check, Figure 2 scatterplots these against the
204 corresponding model climatologies of actual ET; each dot is one grid cell. In almost all the
205 models, our computed PET is a fairly clean, efficient upper bound on the model’s actual ET,
206 as expected from the definition. That is, the most well-watered model grid cells are actually
207 evapotranspiring at rates quite close to our independently computed PET. This success is
208 a rather pleasant surprise considering the very different origins of the two quantities, the
209 models’ use of full Monin-Obukhov surface layer dynamics for C_H , and the potentially large
210 contrast between ASCE-standard alfalfa and the vegetation specified in the model grid cells.

211 **3. Model results**

212 *a. Full PET change*

213 For each of the 13 models and for the multimodel mean, Figure 3 maps the raw % change
214 in climatological annual-mean PET (5) between the 1981-99 and 2081-99 epochs. At each
215 location PET always or almost always increases; that is, ambient conditions become more
216 evaporative with greenhouse warming. This more careful calculation confirms the similar
217 results of Burke et al. (2006), Dai (2013), and Feng and Fu (2013) who quantified this future
218 PET increase only for the mean (or for a single model), and did not resolve the diurnal cycle.
219 In some models a few largely high-latitude regions do see PET decreases or little change in
220 PET, but these are quite localized, and even in these places most models (and the mean)

221 show increases in PET.

222 Furthermore, the magnitude of the projected PET increases is usually in the low double-
223 digits of percent, on the order of 10-45%. In many models certain northern and/or moun-
224 tainous locations see more than this, but over very broad swaths of land these sorts of values
225 are typical. For the multimodel mean, the first row of Table 2 summarizes this by averaging
226 the %-change values over various latitude bands (and subsequent rows similarly average sub-
227 sequent figures.) The magnitudes in Figure 3 agree well with those in Feng and Fu (2013)
228 despite the differing methods. They are also comparable to change magnitudes for annual
229 precipitation P (e.g. Meehl et al. 2007). This further confirms the importance of using
230 P/PET or similar when thinking about the land aridity response to global warming, instead
231 of just P (and/or actual evapotranspiration E , which often contains the same information
232 as P as discussed in section 1a.)

233 In most models and in the mean, there is also a clear tendency toward greater %-increases
234 in PET at higher latitudes (as alluded to above and seen in Table 2), and again Feng and
235 Fu (2013) obtain a similar structure. As far as we know, this basic property has not been
236 explicitly noted in the literature before. (We will see in section 4 that the main reason for
237 this is *not* Arctic amplification of warming.)

238 Yet despite all of these broad commonalities, the models also disagree a great deal, on
239 both the detailed spatial patterns and on the overall magnitude. We will see how these
240 disagreements arise from differences in the climate changes projected by the models.

241 *b. PET changes due to individual factors*

242 Figures 4, 5, 6, and 7 show the %-changes in climatological annual-mean PET (5) that
243 result from perturbing $(R_n - G)$, T_a , RH, and $|u|$ one at a time to 2081-99 levels while keeping
244 the other variables at 1981-99 levels, as explained in detail in section b of the Appendix.
245 One can immediately see here and in Table 2 that the always-positive PET change due to
246 the T_a increase (Figure 5) dominates the other factors in most locations, and explains most

247 of the overall 10-45% magnitude in Figure 3. This is why PET increases are so much more
 248 common than decreases. Again, the physical mechanisms here are widening of the vapor-
 249 pressure deficit by constant-RH increases in e^* , and lowering of the saturated Bowen ratio
 250 by increases in Δ (plus isobaric lowering of ρ_a to a small extent). RH also changes, but the
 251 resulting PET changes (Figure 6) are of both signs, are inconsistent from model to model,
 252 are very weakly positive in the multimodel mean, and are only sporadically (nowhere, in the
 253 mean) negative enough to cancel the T_a -induced increases in Figure 5. This validates the
 254 constant-RH baseline idea, and justifies our decision to think of the vapor-pressure deficit as
 255 $e^*(1 - \text{RH})$ rather than the more customary $(e^* - e_a)$. (An alternative null assumption of
 256 constant vapor pressure deficit would imply systematically increasing RH, which we do not
 257 see.) However, the RH-driven changes can still be very important locally in some models,
 258 explaining the east African PET decrease in BNU-ESM in Figure 3 (for example.)

259 PET changes due to the surface energy supply ($R_n - G$) (Figure 4) are also usually
 260 positive, confirming the physical intuition from section 1b. However, with modal values of
 261 less than 10% (e.g. Table 2) they are generally of secondary importance to the Clausius-
 262 Clapeyron-driven changes (Figure 5) just described. This was not clear a priori - in fact,
 263 some studies in the literature had used radiation changes alone to infer PET changes, as
 264 discussed above in section 1b. As with RH, though, some models have localized regions
 265 where radiation-induced change becomes dominant, e.g. the Amazon Basin in MRI-CGCM3
 266 (and several other models) or the Tibetan Plateau in INM-CM4. (Compare Figures 4, 5 and
 267 3.)

268 In contrast, PET responses to $|u|$ changes (Figure 7) are only rarely important compared
 269 to the other changes. In the multimodel mean and in some individual models (the two
 270 BCC models, CNRM-CM5, and INM-CM4), they are hardly noticeable, usually no larger
 271 than $\pm 5\%$. Like the RH responses (Figure 6) they have no strongly preferred sign, though
 272 decreases are perhaps slightly more common than increases. This is all in stark contrast to
 273 the dominant “stilling” role posited for $|u|$ in the putative recent PET declines, discussed in

274 section 1b.

275 Finally, subtracting the sum of these attributed pieces (Figures 4 through 7) from the
276 full PET change (Figure 3) gives the residual PET change due to nonlinearities, covariance
277 changes, and changes in neglected inputs like p_s . This residual is shown in Figure 8 and is
278 quite weak (0-10%) compared to the T_a -driven or even $(R_n - G)$ -driven changes, though it is
279 usually positive. (The GFDL-CM3 residual at high northern latitudes is a major exception to
280 both of these statements, perhaps because the changes there in Figures 3-6 are all so large.)
281 In any case, we can clearly claim success in our attribution exercise, since the residuals are
282 much smaller than the full changes in Figure 3, and are close to zero for the multimodel
283 mean.

284 Having now examined all of the pieces, we can see that the constant-RH PET response
285 to temperature change (Figure 5) not only explains the general positivity and low-double-
286 digit magnitude of the full PET change, but is also largely responsible for the high-latitude
287 amplification noted in the previous subsection. The response to $(R_n - G)$ (Figure 4) is also
288 polar-amplified, but the temperature response still seems to contain most of the latitudinal
289 contrast shown in Figure 3, as can be clearly seen in Table 2. As for the inter-model
290 disagreement in PET change, responsibility seems to lie with almost all of the terms, but
291 disagreement in the T_a -driven term alone is still large, especially on the overall magnitude.
292 [This makes sense given the well-known disagreement between global climate models on the
293 magnitude of warming in response to an emissions scenario, i.e. transient climate sensitivity
294 (e.g. Meehl et al. 2007).]

295 Therefore, we now attempt a detailed quantitative understanding of the structure and
296 magnitude of this model PET response to ambient temperature change as depicted in Figure
297 5.

298 4. Analytic scaling for the PET response to tempera- 299 ture

300 a. Basic idea

301 How, exactly, is Penman-Monteith PET (5) sensitive to T_a with all else constant? First,
302 one can note that in the numerator of (5) both the aerodynamic term *and* the radiative term
303 increase roughly like Clausius-Clapeyron (C-C) with T_a at constant RH, because $e^*(T)$ is a
304 roughly exponential function and so $\Delta := de^*/dT$ has roughly the same fractional rate of
305 increase with T as e^* does. More precisely (and using the empirical form from Allen et al.
306 (2005) and the Appendix for consistency),

$$e^* = 610.8 \exp\left(\frac{17.27T}{T + 237.3}\right) \quad (6)$$

$$\Delta = \frac{de^*}{dT} = \frac{17.27 \cdot 237.3 \cdot e^*}{(T + 237.3)^2} \quad (7)$$

307 and so,

$$\begin{aligned} \frac{d\Delta}{\Delta dT} &= \frac{d \ln \Delta}{dT} = \frac{d[\ln(17.27 \cdot 237.3) + \ln e^* - 2 \ln(T + 237.3)]}{dT} \\ &= \frac{de^*}{e^* dT} - \frac{2}{T + 237.3} \end{aligned} \quad (8)$$

308 where T is in °C and e^* is in Pa. At Earthlike temperatures $de^*/(e^*dT)$ is around 6-7
309 % deg⁻¹ but $2/(T + 237.3)$ is only 0.7-0.8 % deg⁻¹, so (8) means that $d\Delta/(\Delta dT)$ is not far
310 from $de^*/(e^*dT)$ at all. (These values still hold using the physical C-C equation in place of
311 the empirical (7).) So, all else constant we can expect the entire numerator of PET (5) to
312 increase at a C-C-like rate with warming of T_a , *regardless* of the relative importance of the
313 radiative and aerodynamic terms. This is why we did not further split the response to T_a
314 into responses to e^* and Δ in section 3b above.

315 However, the denominator of (5) cannot necessarily increase so fast: though Δ increases
 316 at roughly C-C as demonstrated, $\gamma(1 + r_s C_H |u|)$ does not depend on T_a *at all*. This term
 317 stops the denominator from fractionally increasing as fast as the numerator, and apparently
 318 is the key reason why PET always increases with T_a (Figure 5) despite the ambiguous sign
 319 of the Δ -driven response discussed in section 1b. If not for the presence of $\gamma(1 + r_s C_H |u|)$,
 320 the denominator would increase about as fast as the numerator, and PET might not be very
 321 sensitive to T_a at all.

322 *b. Derivation and exposition of the scaling*

323 To quantify all of this, we now take the relative partial derivative of (5) with respect to
 324 T_a , repeatedly using the rules

$$\frac{d(a+b)}{a+b} = \frac{da}{a} f_a + \frac{db}{b} f_b \quad (9)$$

325 where $f_a := a/(a+b)$ and $f_b := b/(a+b)$, and

$$\frac{d(a/b)}{a/b} = \frac{da}{a} - \frac{db}{b}, \quad (10)$$

326 plus the chain rule, to yield

$$\frac{d\text{PET}}{\text{PET}} = dT_a \left[\frac{d\Delta}{\Delta dT} f_{rad} + \left(\frac{de^*}{e^* dT} + \frac{d\rho_a}{\rho_a dT} \right) f_{aero} - \frac{d\Delta}{\Delta dT} f_{\Delta} \right]. \quad (11)$$

327 Here f_{rad} is the fraction of the numerator of (5) made up by the radiative term, as in
 328 (9). Similarly, f_{aero} is the fraction of the numerator made up by the aerodynamic term, and
 329 f_{Δ} is the fraction of the denominator of (5) made up by Δ .

330 We then use (8) to write $de^*/(e^* dT)$ in terms of $d\Delta/(\Delta dT)$:

$$\frac{d\text{PET}}{\text{PET}} = dT_a \left[\frac{d\Delta}{\Delta dT} f_{rad} + \left(\frac{d\Delta}{\Delta dT} + \frac{2}{T_a + 237.3} \right) f_{aero} + \frac{d\rho_a}{\rho_a dT} f_{aero} - \frac{d\Delta}{\Delta dT} f_{\Delta} \right]. \quad (12)$$

331 Using $f_{rad} + f_{aero} = 1$ and the ideal-gas-law formula for ρ_a , this reduces to

$$\frac{dPET}{PET} = dT_a \left[\frac{d\Delta}{\Delta dT} (1 - f_\Delta) + \left(\frac{2}{T_a + 237.3} - \frac{1}{T_a + 273.15} \right) f_{aero} \right], \quad (13)$$

332 the main equation that we will use to understand the constant-RH PET response to T_a
 333 as depicted in Figure 5.

334 The first term in the bracket in (13) tells the story laid out in the previous subsection:
 335 the numerator of PET (5) scales like C-C [$d\Delta/(\Delta dT) \cdot 1$] or about 5-6 % deg⁻¹, but the
 336 denominator $\Delta + \gamma(1 + r_s C_H |u|)$ scales closer and closer to C-C the more important Δ is
 337 in it [$-d\Delta/(\Delta dT) \cdot f_\Delta$], weakening the net response. Since Δ is an increasing function of
 338 T_a , this cancellation should occur more (f_Δ should be larger and the denominator should be
 339 more C-C-like) in warmer base climates, so the % sensitivity of PET to T_a should be less
 340 in warmer base climates. We will see in subsection d that this explains the polar-amplified
 341 response pattern in Figure 5. (Similarly, the sensitivity should be greater in windier climates,
 342 in which f_Δ is reduced.)

343 The second term in the bracket in (13) contains the small, miscellaneous departures
 344 from the above: the 0.7-0.8 % deg⁻¹ discrepancy between the scalings of e^* and Δ in the
 345 numerator, and the -0.3-0.4 % deg⁻¹ isobaric dependence of air density on temperature.
 346 The partial cancellation between these two effects makes the net even smaller, ~ 0.4 % deg⁻¹
 347 at the most since f_{aero} can only range between 0 and 1. Therefore, from here on we define
 348 $\epsilon(T) := 2/(T + 237.3) - 1/(T + 273.15)$ and write

$$\frac{dPET}{PET} = dT_a \left[\frac{d\Delta}{\Delta dT} (1 - f_\Delta) + \epsilon(T_a) f_{aero} \right], \quad (14)$$

349 for convenience.

350 *c. From instantaneous to annual-mean scaling*

351 Our equation (14) may be a theory for PET sensitivity at a particular instant. However,
 352 the results from section 3 and Figure 5 that we wish to understand are about annually-
 353 averaged PET. So, to test (14) it is not immediately clear what inputs we should use. For
 354 example, we might use the annual-mean warming $\overline{dT_a}$. (From here on, an overbar will denote
 355 the annual mean.) But if the warming in some place is, say, 6 deg at night but 2 deg during
 356 the day, then using the mean value of 4 deg will overestimate the response because the vast
 357 majority of PET is concentrated during the day when the warming is only 2 deg. So we need
 358 to carefully consider the scaling of the annual mean, $\overline{\overline{\text{PET}}}$, in addition to the instantaneous
 359 PET considered earlier in this section.

360 The relative change in $\overline{\overline{\text{PET}}}$ turns out to be the *PET-weighted average* of the relative
 361 change in instantaneous PET. This is because, again, the more PET is concentrated at a
 362 particular time, the more a % change in PET at that time matters to the % change in $\overline{\overline{\text{PET}}}$.
 363 Mathematically,

$$\frac{d\overline{\overline{\text{PET}}}}{\overline{\overline{\text{PET}}}} = \frac{d\overline{\text{PET}}}{\overline{\text{PET}}} = \frac{\overline{(d\text{PET}/\text{PET}) \text{PET}}}{\overline{\text{PET}}} := \overline{\overline{(d\text{PET}/\text{PET})}} \quad (15)$$

364 where from here on a double overbar denotes a PET-weighted annual average, $\overline{\overline{a}} :=$
 365 $\overline{a \cdot \text{PET}}/\overline{\text{PET}}$ for any variable a . So, using (14):

$$\frac{d\overline{\overline{\text{PET}}}}{\overline{\overline{\text{PET}}}} = \overline{\overline{dT_a \left[\frac{d\Delta}{\Delta dT} (1 - f_\Delta) + \epsilon(T_a) f_{aero} \right]}}. \quad (16)$$

366 Essentially, we need to evaluate (14) at times of the day and year when PET is large.
 367 This suggests the following simple approximation to (16):

$$\frac{d\overline{\overline{\text{PET}}}}{\overline{\overline{\text{PET}}}} \approx \overline{\overline{dT_a}} \left[\frac{d\Delta}{\Delta dT} \left(\overline{\overline{T_a}} \right) \left(1 - \overline{\overline{f_\Delta}} \right) + \epsilon \left(\overline{\overline{T_a}} \right) \overline{\overline{f_{aero}}} \right]. \quad (17)$$

368 *d. Testing the annual-mean scaling*

369 To test this scaling theory (17), we compute $\overline{dT_a} = \overline{dT_a \cdot \text{PET}} / \overline{\text{PET}}$, $\overline{f_\Delta} = \overline{f_\Delta \cdot \text{PET}} / \overline{\text{PET}}$,
 370 and so forth for each model grid-cell. For the base-state variables PET, f_Δ , and T_a , we just
 371 use diurnally and annually varying 1981-99 climatologies computed as in section 2, not the
 372 full 19-year time series. Similarly, for the change dT_a , we use the same smoothed diurnally
 373 and annually varying climatological difference that we used to produce Figure 5, as detailed
 374 in section b of the Appendix. (Note that $\overline{f_{aero}}$ turns out to simply be the fraction of annual-
 375 total PET that comes from the aerodynamic term, so we compute aerodynamic and radiative
 376 $\overline{\text{PET}}$ separately, and directly use this fraction.)

377 Since $d\Delta / (\Delta dT)$ is not that dependent on temperature and $\epsilon \overline{f_{aero}}$ is small, the main
 378 sensitivity wild-card in (17) should be $\overline{f_\Delta}$, the fraction of the denominator of (5) made up by
 379 Δ at high-PET times of day and year. $\overline{f_\Delta}$ determines whether the denominator will keep up
 380 with the numerator's Clausius-Clapeyron pace and curtail the PET increase with warming,
 381 or lag behind it and allow a large PET increase.

382 So, in Figure 9 we map $\overline{f_\Delta}$ for each model, as well as the multimodel mean of $\overline{f_\Delta}$ (sum-
 383 marized in Table 2, as above.) One can see that it dramatically varies from as low as ~ 0.25
 384 in the cool-summer climates of the coastal high latitudes, to ~ 0.75 in the warm climates
 385 of the tropics. Apparently the strong dependence of Δ on temperature is in control of this
 386 fraction, even though it also depends on quantities in the denominator's other term ($|u|$ and
 387 our daylength-dependent r_s .) Indeed, Figure 10 shows that the PET-weighted (i.e. daytime,
 388 warm-season) basic-state temperature $\overline{T_a}$ has a strikingly similar spatial pattern to this $\overline{f_\Delta}$,
 389 often even at very fine spatial scales. Essentially, in cool, low- Δ climates the denominator
 390 of (5) is mainly made up of $\gamma(1 + r_s C_H |u|)$ which stays fixed with T_a and lets (5) increase,
 391 while in warm climates it is dominated by Δ , which scales like C-C and cancels most of the
 392 numerator's attempt to increase PET.

393 Figure 11 then maps the entire bracketed term from (17), i.e. our scaling estimate of
 394 the % sensitivity of $\overline{\text{PET}}$ to PET-weighted warming. As guessed, its pattern is nearly the

395 same as that of $\overline{f_{\Delta}}$ (Figure 9) [and thus $\overline{T_a}$ (Figure 10)], varying from around 1.5 % deg⁻¹
 396 over large areas of the planet’s warm, high- $\overline{f_{\Delta}}$ tropics, to nearly C-C in the coolest-summer
 397 regions where $\overline{f_{\Delta}}$ is small and the numerator in (5) can increase nearly unopposed. The
 398 models agree on all of these fields much more than they agree on the gross response to T_a
 399 change depicted in Figure 5. This is not surprising, since these are only based on properties
 400 of the models’ 1981-99 base climates, which can be tuned to match observations.

401 On the other hand, the PET-weighted projected warming $\overline{dT_a}$ (the other factor in (17))
 402 might vary considerably from model to model, since the models do not agree on the warming
 403 response to a given greenhouse-gas forcing scenario (e.g. Meehl et al. 2007). Figure 12 maps
 404 $\overline{dT_a}$ for each model and for the mean, confirming that the spread in modeled warming is
 405 much larger than the spread in estimated sensitivity to that warming (Figure 11). Taking
 406 the end members, $\overline{dT_a}$ over land seems to be almost 3 times stronger in GFDL-CM3 than in
 407 INM-CM4! Thus it appears that the main reason for the inter-model spread in the magnitude
 408 of the $\overline{\text{PET}}$ change due to warming (Figure 5), noted in section 3b, is indeed the inter-model
 409 spread in the warming itself.

410 We are also now in a position to evaluate the source of the high-latitude amplification of
 411 the $\overline{\text{PET}}$ %-change pattern in Figure 5, and thus in Figure 3. Figure 12 shows that the PET-
 412 weighted warming $\overline{dT_a}$ is indeed strongly Arctic-amplified in some models, e.g. BNU-ESM
 413 and GFDL-CM3. However, in many other models this pattern is absent, even though it is
 414 well known that the Arctic amplification of the *annual-mean* warming $\overline{dT_a}$ is robust across
 415 climate models (e.g. Meehl et al. 2007). For example, in ACCESS1.0 $\overline{dT_a}$ maximizes in
 416 mid-latitude North America and Europe and in the Amazon Basin, and in GFDL-ESM2G
 417 and GFDL-ESM2M $\overline{dT_a}$ maximizes in the subtropics. So $\overline{dT_a}$ does not consistently show
 418 high-latitude amplification, and in the multimodel mean any such amplification is quite
 419 weak (Figure 12; Table 2). This is probably because high-latitude warming amplification is
 420 more of a cold-season than a warm-season phenomenon (Meehl et al. 2007), while a PET-
 421 weighted mean is largely over the warm season. In contrast, the sensitivity factor in (17),

422 depicted in Figure 11, shows strong and systematic high-latitude amplification because of the
 423 strong control of $\overline{f_\Delta}$ (Figure 9) by the basic-state temperature $\overline{T_a}$ (Figure 10), as discussed
 424 above. Thus it appears that $d\overline{\text{PET}}/\overline{\text{PET}}$ (Figures 5 and 3) is polar-amplified not because
 425 the warming is polar-amplified, but largely because colder climates with Δ less important in
 426 the denominator of PET are inherently more sensitive. (Compare the last two lines of Table
 427 2.)

428 Finally, we can confirm this picture by evaluating (17) and comparing to the model $\overline{\text{PET}}$
 429 responses to T_a changes in Figure 5. Before displaying the result, we need to note that if
 430 the sensitivity factor in (17) is, e.g., 4 % deg⁻¹ and the projected warming $\overline{dT_a}$ is 9 deg, the
 431 expected $\overline{\text{PET}}$ change should be noticeably larger than 36% because $1.04^9 \approx \exp(0.36) >$
 432 1.36. To account for this simple nonlinearity, we exponentiate (17) and subtract 1 to arrive
 433 at our final scaling guess for what Figure 5 should look like.

434 This estimate is shown in Figure 13, and is strikingly close to the model response in
 435 Figure 5. In fact, the summary values in Table 2 differ from the actual values on the line
 436 above by only about +1% (of the basic state; about 10% of the changes.) Thus, we can
 437 claim success in understanding the magnitude, structure and inter-model spread in Figure
 438 5. The low double-digit % magnitude of $d\overline{\text{PET}}/\overline{\text{PET}}$ comes from the mid-single-digit °C
 439 greenhouse warming (Figure 12) times the sub-Clausius-Clapeyron, 1-4.5% deg⁻¹ sensitivity
 440 of (5) at constant RH (Figure 11 and sections 4a-b). The structure of $d\overline{\text{PET}}/\overline{\text{PET}}$ comes
 441 mainly from the structure of the base-climate temperature $\overline{T_a}$ (Figure 10) via $\overline{f_\Delta}$ (Figure 9)
 442 and the sensitivity, and also somewhat from the structure of the warming. The inter-model
 443 spread comes from the inter-model spread in the warming.

444 5. Sensitivity of results to imposed vegetation

445 One might wonder whether the above holds for parameter choices in (5) other than
 446 the ones presented in section 2 and the Appendix. In particular, the transfer coefficient

447 C_H and bulk stomatal resistance r_s could potentially modulate the T_a -independent term
 448 $\gamma(1 + r_s C_H |u|)$ in the denominator of (5), and therefore alter $\overline{f_\Delta}$ and the bracketed sen-
 449 sitivity in (17). So, we also compute results using a few alternative choices for these two
 450 parameters.

451 We first examine the effect of setting $r_s \equiv 0$, i.e. neglecting the relatively small but
 452 appreciable stomatal resistance of well-watered transpiring leaves, as in many formulations
 453 of Penman-Monteith PET including those used by Burke et al. (2006), Dai (2013), and Feng
 454 and Fu (2013), as well as in the case of pan evaporation. This gives an expression more in
 455 the spirit of Penman (1948) than Monteith (1981): the denominator of (5) simply becomes
 456 $\Delta + \gamma$. This choice should systematically increase f_Δ and thus reduce the % change in $\overline{\text{PET}}$
 457 (by (17)), taking it even further from Clausius-Clapeyron. Indeed, the range of $\overline{f_\Delta}$ shifts
 458 upward, to roughly 0.4-0.85 (not shown). However, the original range in Figure 9 was about
 459 0.25-0.75, so this is a quantitative but not a qualitative increase. The spatial pattern of $\overline{f_\Delta}$
 460 hardly changes, except for losing some fine-scale structure due to the loss of $|u|$ dependence.

461 Figure 14 shows the % changes in PET from changing T_a in this case. Comparison with
 462 the analogous Figure 5 shows that setting $r_s \equiv 0$ indeed weakens the response, making single-
 463 digit-% values somewhat more common and values > 30 % less common, but the patterns are
 464 very close. The at-a-point differences between the two figures are much less than the spatial
 465 and model-to-model variations within each figure, and the summary statistics in Table 2
 466 differ by only about 2-3% (of the basic state.)

467 We also examine a “smooth” version of (5), in which the 0.5 m vegetation height h and
 468 thus the roughness lengths z_{om} and z_{oh} in (A1) are reduced by a factor of 10, setting h to a
 469 grass-like 5 cm and halving C_H from $\approx 5.7 \times 10^{-3}$ to $\approx 2.8 \times 10^{-3}$. (The Penman-Monteith
 470 formulations used in Burke et al. (2006), Dai (2013), and Feng and Fu (2013) also assume a
 471 smoother surface.) This, too, shifts the range of $\overline{f_\Delta}$ only slightly upward, to roughly 0.35-0.8,
 472 with a very similar spatial pattern to the original in Figure 9. So, the % change in $\overline{\text{PET}}$
 473 ends up looking almost identical to Figure 5, but slightly (several %) weaker (not shown).

474 Again, the parameter-induced alterations in $\overline{dPET}/\overline{PET}$ are much less than the spatial and
475 model-to-model variation.

476 Also, in the no-resistance case, adding this “smooth” vegetation would not appreciably
477 lower the results any further, because in that case C_H does not even appear in the de-
478 nominator of (5), and thus can no longer affect $\overline{f_\Delta}$. Thus, the effects are not additive –
479 the no-resistance case gives a strict upper bound on $\overline{f_\Delta}$ and an effective lower bound on
480 warming-induced $\overline{dPET}/\overline{PET}$ (Figure 14).

481 Finally, we examine a “rough”, forest-like PET in which h , z_{om} and z_{oh} are *increased* by
482 a factor of 10, setting h to 5 m and tripling C_H to $\approx 1.7 \times 10^{-2}$, a very large value. In
483 this case, the range of $\overline{f_\Delta}$ falls to roughly 0.15-0.7, again with a very similar spatial pattern
484 to Figure 9. $\overline{dPET}/\overline{PET}$ from T_a becomes somewhat larger than shown in Figure 5, with
485 values of 35-40% or more becoming more widespread. But again there is little qualitative
486 or pattern change; the overall story is the same. In summary, widely different choices of
487 vegetation parameters do not alter the big picture presented in sections 3 and 4 above.

488 There is also the question of whether r_s , like $(R_n - G)$, T_a , RH, $|u|$ (and p_s), should
489 have been treated as changing between the two epochs rather than staying fixed. After
490 all, the carbon dioxide increase that causes greenhouse warming may also cause individual
491 plant stomata to close (e.g. Sellers et al. 1996). However, there is still very large uncertainty
492 about the bulk vegetation changes that will occur in concert with this, much larger than
493 the uncertainty in the *climate* response to carbon dioxide (Huntingford et al. 2013). Almost
494 nothing is known about this bulk response. Furthermore, the % sensitivity of Penman-
495 Monteith PET (5) to a % change in r_s turns out to depend very strongly on the vegetation
496 parameters r_s and C_D , in contrast to the much weaker dependence just presented in the case
497 of sensitivity to T_a . Therefore, in this study we decided to only scale the PET response to
498 climate change, and not the response to carbon-dioxide-induced plant physiological change.

6. Summary and discussion

Potential evapotranspiration (PET), the rate at which surface water evaporates if available in a given climate, has been projected to increase with future greenhouse warming in most or all locations, driving strong global trends toward drought (e.g. Dai 2013; Burke et al. 2006) and/or aridity (Feng and Fu 2013). In this study, we systematically analyzed the projected response of the Penman-Monteith equation (5), the fundamental physical quantification of PET used by those studies. We found that, at least in the 13 modern global climate models listed in Table 1, the main reason for the projected PET increase is the warming itself (Figure 5), not the greenhouse-driven increase in surface net radiation (Figure 4). The warming causes the PET increase by widening the vapor pressure deficit $e^*(1 - \text{RH})$ corresponding to a given relative humidity RH, and/or by increasing the local slope $\Delta := de^*/dT$ of the Clausius-Clapeyron curve which governs the partitioning between sensible and latent heat fluxes. Changes in RH are not of any strongly preferred sign and are not large enough to alter this.

The magnitude of the projected annual-mean PET increase between 1981-99 and a business-as-usual 2081-99 scenario is usually a low double-digit percentage (Figures 5 and 3; Table 2), comparable to projections for local precipitation. This is because the numerator of the Penman-Monteith equation (5) increases like Clausius-Clapeyron (5-6 % deg^{-1}) with constant-RH warming, but in the denominator only the first term Δ increases similarly, while the second term stays fixed. Thus, the net response of (5) to warming is sub-Clausius-Clapeyron, usually about 1.5-4 % deg^{-1} (Figure 11). The higher values are found in cooler climates where Δ is smaller and thus less important in the denominator of (5) (i.e. $\overline{f_\Delta}$ in (17) is smaller), and the lower values are found in warmer climates, explaining the strongly polar-amplified change pattern. Since the projected PET-weighted-mean warming for this scenario tends to be in the single digits of $^\circ\text{C}$ in most places (Figure 12), the gross % response of PET to warming ends up in the lower double digits (Figure 5; Figure 13). Large disagreement between models on the exact amount of warming produces similar disagree-

526 ment on the total PET response. (The smaller but appreciable radiation- and RH-driven
 527 PET change components shown in Figures 4 and 6 also vary widely between models, adding
 528 to the disagreement.)

529 A key further advantage of our scaling approach (17) is that a climate model is not even
 530 needed for a user to locally compute the sensitivity of PET to future warming. All variables
 531 inside the square brackets in (17) can be computed during routine calculations of observed
 532 present-day Penman-Monteith PET. For example, the values of $f_{\Delta} = \Delta / (\Delta + \gamma (1 + r_s C_H |u|))$
 533 and PET can be noted at each calculation time-step and averaged over several years of data
 534 collection to obtain seasonally and/or diurnally resolved climatologies, which can then be
 535 used to find $\overline{f_{\Delta}} = \overline{f_{\Delta} \cdot \text{PET}} / \overline{\text{PET}}$. If it turns out that $\overline{f_{\Delta}}$ can be accurately estimated
 536 straight from Δ ($\overline{T_a}$) and $\overline{|u|}$, then the computation will be even simpler, as there will be
 537 no need to archive short-term values of f_{Δ} . So, whether the sensitivities plotted in Figure
 538 11 contain model biases is not actually that important for the practical use of (17).

539 We would also like to briefly give a more qualitative, physical explanation for why PET
 540 is less sensitive to T_a in warmer base climates. First, consider a climate cold enough that
 541 LH is unimportant in (3) even under well-watered conditions, and the dominant balance is
 542 between SH and $(R_n - G)$. In this climate, fixing $(R_n - G)$ effectively fixes SH, which fixes
 543 $(T_s - T_a)$ by (1). Now, if we rewrite (2) with the substitutions introduced later in section
 544 1b,

$$\text{LH} = \frac{\rho_a c_p (\Delta (T_s - T_a) + e^* (1 - \text{RH}))}{\gamma (r_s + r_a)}, \quad (18)$$

545 we can see that LH will be able to increase at Clausius-Clapeyron, driven by Δ and e^* .
 546 Everything else in (18) is fixed by assumption. However, as the climate warms and well-
 547 watered LH becomes appreciable, the evaporation will start to cool T_s relative to T_a and limit
 548 the fractional increase of (18). (Eventually, energy conservation (3) will start to severely
 549 limit the increase in well-watered LH, since $(R_n - G)$ is fixed here, and $(T_s - T_a)$ and SH
 550 can only go so negative due to constraints involving the wet-bulb depression associated with

551 our fixed RH.)

552 We also note that the PET % responses to changes in $(R_n - G)$, RH, and $|u|$, depicted
553 in Figures 4, 6, and 7, can also be analytically scaled in the manner demonstrated for T_a in
554 section 4, with similar levels of success. However, the modeled changes in these variables (for
555 input to these scalings) are not as well-understood as the modeled warming dT_a , so these
556 scalings do not provide as much understanding.

557 Finally, we are still interested in under what conditions or assumptions this large sys-
558 tematic PET increase with climate warming actually implies a systematic drying-out of the
559 land, as suggested by much of the work cited in section 1. To this end, we also have work in
560 progress testing the sensitivity of modeled soil moisture to large changes in global tempera-
561 ture across a very wide range of continental geographies, forcing mechanisms, and land and
562 atmospheric modeling choices.

563 *Acknowledgments.*

564 The lead author would like to thank A. Dai for providing results on drought projections
565 using different PET methods, and A. Swann for a key suggestion on section 4b. The authors
566 also acknowledge the World Climate Research Programme’s Working Group on Coupled
567 Modelling, which is responsible for CMIP, and we thank the climate modeling groups (listed
568 in Table 1) for producing and making available their model output. For CMIP the U.S.
569 Department of Energy’s Program for Climate Model Diagnosis and Intercomparison provides
570 coordinating support and led development of software infrastructure in partnership with the
571 Global Organization for Earth System Science Portals. This work was supported by NSF
572 grants AGS-0846641 and AGS-0936059.

573

574

Detailed methods

575

576 *a. Parameter and procedural choices for the Penman-Monteith equation*

577 Allen et al. (2005) provide parameters for two different reference vegetation types: short
 578 clipped grass, and alfalfa (with the expectation that “crop coefficients” will be determined for
 579 conversion of the resulting PET output to values suitable for other vegetation.) We use the
 580 alfalfa values, reasoning that natural vegetation is closer to alfalfa in roughness and leafiness
 581 than it is to short clipped grass. Similarly, procedures are standardized separately for hourly
 582 and for daily calculation time-steps; we use the hourly procedures on the 3-hourly model
 583 intervals. For meteorological variables, the model output is given as synoptic “snapshots”
 584 every 3 hours, so for each interval we average the initial and final values of T_a , specific
 585 humidity q_a , and $|u|$ to estimate 3-hour means, analogous to the hour means used by Allen
 586 et al. (2005). [Note that the raw output includes the wind components u and v but not the
 587 speed $|u|$, so $|u|$ has to be computed as $\sqrt{u^2 + v^2}$ at each snapshot before this averaging step.
 588 Also, 2 of the models (see Table 1) give u and v on a grid staggered by one-half the spacing
 589 in latitude and longitude from the main grid used for all the other variables, so we compute
 590 u at each main gridpoint as the mean of u at the 4 surrounding wind-gridpoints, and similar
 591 for v , before this computation of $|u|$.]

592 With these choices of time-step and vegetation types, the ASCE standardized procedures
 593 for variables in (5), and our few departures from them, are given as follows. A constant p_s
 594 is hydrostatically estimated from the surface elevation, but for simplicity we directly use the
 595 3-hourly p_s output from the model, averaged like T_a and q_a above. e^* is computed from the
 596 (3)-hour-mean T_a using the empirical form $e^*(T) = 610.8 \exp(17.27T/(T + 237.3))$, where
 597 e^* is in Pa and T is in °C, and Δ using its derivative. ρ_a is computed from the dry-air

598 ideal gas law, using the (3)-hour-mean T_a multiplied by 1.01 to account for virtual effects. A
 599 number of standardized methods are given to compute e_a from measurements; we directly use
 600 the 3-hour-mean model q_a above, multiplying by p_s/ε to convert the units (nearly identical
 601 to their Method No. 1.) RH can then be computed as e_a/e^* . (In a few models this RH can
 602 occasionally slightly exceed 1, presumably due to interpolation; in these cases we set RH = 1
 603 to avoid unphysical negative values of the aerodynamic term.) L_v is idealized as a constant
 604 $2.45 \times 10^6 \text{ J kg}^{-1}$. A field estimation method for R_n and a simple parameterization of G are
 605 given, but we simply compute $(R_n - G)$ from the model-output actual turbulent heat fluxes
 606 SH and LH using (3), which is still valid. These fluxes are already provided as 3-hour means
 607 over our intervals, so there is no need for averaging. r_s is then set at 30 s m^{-1} (“open”)
 608 during the day and 200 s m^{-1} (“closed”) at night, where “day” and “night” are defined as
 609 $R_n > 0$ and $R_n < 0$. We use $(R_n - G) > 0$ and $(R_n - G) < 0$ instead; this is justified since
 610 Allen et al. (2005) parameterize G as a small positive fraction of R_n .

611 For the transfer coefficient C_H , the standardized choice is the neutral, log-layer form,

$$C_H = \frac{k^2}{\ln((z_w - d)/z_{om}) \ln((z_h - d)/z_{oh})} \quad (\text{A1})$$

612 where k is von Karman’s constant, z_w is the height of the windspeed measurements,
 613 z_{om} is the momentum roughness length, z_h is the height of the temperature and humidity
 614 measurements, z_{oh} is the scalar roughness length, and d is the zero-plane displacement.
 615 Allen et al. (2005) do not attempt to justify this choice, but one could argue that the great
 616 majority of PET is in warmer seasons or climates during the daytime, when the surface
 617 layer is either neutral or convective. For most windspeeds the Monin-Obukhov correction
 618 to C_H for convective conditions is much smaller than for stable conditions, so the worst of
 619 the potential problems are avoided. In any case, the standardized values for (A1) are as
 620 follows: k is set to 0.41. z_w and z_h are each set to 2 m, though we use 10 m for z_w to
 621 match the height of the model wind output. If h is the assumed vegetation height (0.5 m
 622 for our standard alfalfa choice), z_{om} is set to $0.123h$, and z_{oh} to $0.0123h$. Finally, d is set

623 to 0.08 m on the assumption that the weather measurements are taken over clipped grass,
624 but we conservatively set $d = 0$ as it is not clear what exactly the model output heights are
625 measured relative to. With these choices, C_H works out to $\approx 5.7 \times 10^{-3}$.

626 *b. Determining the PET responses to individual variables*

627 We would like to isolate the PET changes due to changes in the individual inputs
628 $(R_n - G)$, T_a , RH, and $|u|$. However, we cannot simply give (5) the 2081-99 time series
629 for one of these and the 1981-99 time series for all other variables, because the differing
630 synoptic histories of the two epochs would destroy any inter-input correlations other than
631 the diurnal and annual cycles, adding an artificial change to the result. So, for each of these
632 four inputs, we compute diurnally and annually varying climatologies for each model (as
633 for PET), further smooth them with a 7-day running mean that respects the diurnal cycle,
634 difference the two epochs (divide them, in the case of $|u|$), and perturb each year of the
635 1981-99 input time series by this diurnally and annually varying difference (factor), creating
636 an input time series with the climatological properties of 2081-99 but the synoptic history of
637 1981-99. These can then be used one at a time in (5) to isolate the responses to $(R_n - G)$,
638 T_a , RH, and $|u|$. [When we perturb $(R_n - G)$, we still use the original 1981-99 $(R_n - G)$
639 series to define day and night for setting r_s . Global warming may accomplish many feats,
640 but it certainly will not transmute night into day! Consistent with this, when computing the
641 2081-2099 PET in section 2, we subtract our diurnally and annually varying climatological
642 difference from each year of the 2081-2099 $(R_n - G)$ series before it is used to define night
643 and day.]

REFERENCES

- 646 Allen, R. G., I. A. Walter, R. Elliott, T. Howell, D. Itenfisu, and M. Jensen, 2005: *The ASCE*
647 *Standardized Reference Evapotranspiration Equation*. American Society of Civil Engineers,
648 59 pp.
- 649 Arora, V. K., 2002: The use of the aridity index to assess climate change effect on annual
650 runoff. *J. Hydrol.*, **265**, 164–177.
- 651 Brutsaert, W. and M. B. Parlange, 1998: Hydrologic cycle explains the evaporation paradox.
652 *Nature*, **396**, 30.
- 653 Budyko, M. I. and D. H. Miller, 1974: *Climate and Life*. Academic Press, 508 pp.
- 654 Burke, E. J., S. J. Brown, and N. Christidis, 2006: Modeling the recent evolution of global
655 drought and projections for the twenty-first century with the Hadley Centre climate model.
656 *J. Hydrometeor.*, **7**, 1113–1125.
- 657 Dai, A., 2013: Increasing drought under global warming in observations and models. *Nature*
658 *Clim. Change*, **3**, 52–58, doi:10.1038/NCLIMATE1633.
- 659 Feng, S. and Q. Fu, 2013: Expansion of global drylands under warming climate. *Atmos.*
660 *Chem. Phys.*, in press.
- 661 Hartmann, D., 1994: *Global Physical Climatology*. Academic Press, 411 pp.
- 662 Held, I. and B. Soden, 2006: Robust responses of the hydrological cycle to global warming.
663 *J. Climate*, **19**, 5686–5699.
- 664 Held, I. M. and B. J. Soden, 2000: Water vapor feedback and global warming. *Annu. Rev.*
665 *Energy Environ.*, **25**, 441–475, doi:10.1146/annurev.energy.25.1.441.

- 666 Hobbins, M. T., A. Dai, M. L. Roderick, and G. D. Farquhar, 2008: Revisiting the parame-
667 terization of potential evaporation as a driver of long-term water balance trends. *Geophys.*
668 *Res. Lett.*, **35**, L12403, doi:10.1029/2008GL033840.
- 669 Huntingford, C., et al., 2013: Simulated resilience of tropical rainforests to CO₂-induced
670 climate change. *Nature Geoscience*, **6**, 268–273, doi:10.1038/ngeo1741.
- 671 Lofgren, B. M., T. S. Hunter, and J. Wilbarger, 2011: Effects of using air temperature as
672 a proxy for potential evapotranspiration in climate change scenarios of Great Lakes basin
673 hydrology. *J. Great Lakes Res.*, **37**, 744–752, doi:10.1016/j.jglr.2011.09.006.
- 674 McKenney, M. S. and N. J. Rosenberg, 1993: Sensitivity of some potential evapotranspiration
675 estimation methods to climate change. *Agric. For. Meteorol.*, **64**, 81–110.
- 676 McVicar, T. R., T. G. V. Niel, L. T. Li, M. L. Roderick, D. P. Rayner, L. Ricciardulli,
677 and R. J. Donohue, 2008: Wind speed climatology and trends for Australia, 1975-2006:
678 capturing the stilling phenomenon and comparison with near-surface reanalysis output.
679 *Geophys. Res. Lett.*, **36**, L20403, doi:10.1029/2008GL035627.
- 680 McVicar, T. R., et al., 2012: Global review and synthesis of trends in observed terrestrial
681 near-surface wind speeds: implications for evaporation. *J. Hydrol.*, **416-417**, 182–205,
682 doi:10.1016/j.jhydrol.2011.10.024.
- 683 Meehl, G. A., et al., 2007: Global climate projections. *Climate Change 2007: The Physical*
684 *Science Basis. Contribution of Working Group I to the Fourth Assessment Report of the*
685 *Intergovernmental Panel on Climate Change*, S. Solomon, D. Qin, M. Manning, Z. Chen,
686 M. Marquis, K. B. Averyt, M. Tignor, and H. L. Miller, Eds., Cambridge University Press,
687 747–845.
- 688 Middleton, N. and D. S. G. Thomas, 1997: *World Atlas of Desertification*. 2d ed., Wiley,
689 182 pp.

- 690 Monteith, J. L., 1981: Evaporation and surface temperature. *Q. J. R. Meteorol. Soc.*, **107**,
691 1–27.
- 692 Mortimore, M., 2009: *Dryland Opportunities: A new paradigm for people, ecosys-*
693 *tems and development*. IUCN, IIED, and UNDP/DDC, 86 pp., [Available online at
694 pubs.iied.org/pdfs/G02572.pdf].
- 695 Palmer, W. C., 1965: Meteorological drought. U.S. Weather Bureau Research Paper 45, 58
696 pp.
- 697 Penman, H. L., 1948: Natural evaporation from open water, bare soil and grass. *Proc. R.*
698 *Soc. Lond. A*, **193**, 120–145, doi:10.1098/rspa.1948.0037.
- 699 Price, C. and D. Rind, 1994: The impact of a 2xCO₂ climate on lightning-caused fires. *J.*
700 *Clim.*, **7**, 1484–1494.
- 701 Pryor, S. C., et al., 2009: Wind speed trends over the contiguous United States. *J. Geophys.*
702 *Res.*, **114**, D14105, doi:10.1029/2008JD011416.
- 703 Rind, D., R. Goldberg, J. Hansen, C. Rosenzweig, and R. Ruedy, 1990: Potential evapo-
704 transpiration and the likelihood of future drought. *J. Geophys. Res.*, **95**, 9983–10 004.
- 705 Roderick, M. L., M. T. Hobbins, and G. D. Farquhar, 2009: Pan evaporation trends and
706 the terrestrial water balance. II. Energy balance and interpretation. *Geog. Compass*, **3/2**,
707 761–780, doi:10.1111/j.1749-8198.2008.00214.x.
- 708 Seager, R., et al., 2007: Model projections of an imminent transition to a more arid climate
709 in southwestern North America. *Science*, **316**, 1181–1184, doi:10.1126/science.1139601.
- 710 Sellers, P., et al., 1996: Comparison of radiative and physiological effects of doubled atmo-
711 spheric CO₂ on climate. *Science*, **271**, 1402–1406.
- 712 Taylor, K. E., R. J. Stouffer, and G. A. Meehl, 2012: An overview of CMIP5 and the exper-
713 iment design. *Bull. Amer. Meteorol. Soc.*, **93**, 485–498, doi:10.1175/BAMS-D-11-00094.1.

- 714 Thornthwaite, C. W., 1948: An approach toward a rational classification of climate. *Geog.*
715 *Rev.*, **38**, 55–94.
- 716 Wang, K., R. E. Dickinson, and S. Liang, 2012: Global atmospheric evaporative demand
717 over land from 1973 to 2008. *J. Climate*, **25**, 8353–8361, doi:10.1175/JCLI-D-11-00492.1.
- 718 Wehner, M., D. R. Easterling, J. H. Lawrimore, R. R. Heim, R. S. Vose, and B. D. San-
719 ter, 2011: Projections of future drought in the continental United States and Mexico. *J.*
720 *Hydrometeor.*, **12**, 1359–1377, doi:10.1175/2011JHM1351.1.

721 **List of Tables**

722	1	CMIP5 models analyzed in this study	33
723	2	Results for the multimodel mean, averaged over different latitude bands	34

TABLE 1. CMIP5 models analyzed in this study

Model name	ID on figures	Modeling group
ACCESS1.0 ¹	access	Commonwealth Scientific and Industrial Research Organization (CSIRO) and Bureau of Meteorology (BOM), Australia
BCC-CSM1.1	bcc	Beijing Climate Center, China Meteorological Administration
BCC-CSM1.1-M	bccm	
BNU-ESM	bnu	College of Global Change and Earth System Science, Beijing Normal University
CNRM-CM5	cnrm	Centre National de Recherches Météorologiques / Centre Européen de Recherche et Formation Avancées en Calcul Scientifique, France
GFDL-CM3	gfdl3	NOAA Geophysical Fluid Dynamics Laboratory, USA
GFDL-ESM2G	gfdleg	
GFDL-ESM2M	gfdlem	
HadGEM2-ES ¹²³	had	Met Office Hadley Centre, United Kingdom
INM-CM4	inm	Institute for Numerical Mathematics, Russia
IPSL-CM5A-LR	ipsll	Institut Pierre-Simon Laplace, France
IPSL-CM5A-MR	ipslm	
MRI-CGCM3	mri	Meteorological Research Institute, Japan

¹Surface winds were given on a grid staggered from that of the other surface variables; see section a of the Appendix.

²Run 2 was used for historical (and run 1 was used for rcp8.5), as these were the only respective runs with 3-hourly output.

³3-hourly surface pressure was not available, so monthly surface pressure output was used for each 3-hour interval.

TABLE 2. Results for the multimodel mean, averaged over different latitude bands

Fig.	Quantity	60-15°S	15°S-15°N	15-40°N	40-80°N
3	% change in PET	16.9	14.0	17.8	24.4
4	% change in PET due to $(R_n - G)$	1.7	3.0	2.6	5.1
5	% change in PET due to T_a	9.7	7.1	12.5	17.6
13	% change in PET due to T_a (Scaling)	10.6	7.7	13.5	19.1
6	% change in PET due to RH	3.4	1.9	1.8	2.5
7	% change in PET due to $ u $	1.0	0.7	0.1	-0.7
8	% change in PET (residual)	1.0	1.3	0.8	-0.2
14	% change in PET due to T_a if $r_s \equiv 0$	7.0	5.4	9.0	15.2
10	PET-weighted-mean T_a , °C	24	27	23	13
9	PET-weighted-mean f_Δ (see section 4)	0.61	0.69	0.59	0.48
11	Analytic PET sensitivity to T_a , % deg ⁻¹	2.2	1.7	2.4	3.2
12	PET-weighted-mean warming, deg	4.5	4.4	5.2	5.5

724 List of Figures

- 725 1 1981-99 climatological annual-mean Penman-Monteith PET (5) in mm day^{-1}
726 for each CMIP5 model in Table 1. Last panel is the mean over all applicable
727 models (omitting locations where less than half of the models were analyzed.) 37
- 728 2 1981-99 climatological annual-mean actual ET (vertical, $0-6 \text{ mm day}^{-1}$) vs.
729 PET (horizontal, $0-13 \text{ mm day}^{-1}$) for each model, where each dot is one grid
730 cell. Red lines are 1:1 (actual ET = PET.) 38
- 731 3 % changes in climatological annual-mean PET between 1981-99 and 2081-99,
732 for each model. (Values in a few color-saturated regions greatly exceed those
733 on the scale.) Last panel is the % change in the multimodel mean. 39
- 734 4 % changes in climatological annual-mean PET from setting only the surface
735 radiative energy supply ($R_n - G$) to 2081-99 levels while leaving all other
736 variables in (5) at 1981-99 levels. 40
- 737 5 % changes in climatological annual-mean PET from setting only the ambient
738 air temperature T_a (and thus the saturation vapor pressure e^* and its deriva-
739 tive Δ) to 2081-99 levels while leaving all other variables in (5), including
740 relative humidity RH, at 1981-99 levels. 41
- 741 6 % changes in climatological annual-mean PET from setting only the relative
742 humidity RH to 2081-99 levels while leaving all other variables in (5) at 1981-
743 99 levels. 42
- 744 7 % changes in climatological annual-mean PET from setting only the wind-
745 speed $|u|$ to 2081-99 levels while leaving all other variables in (5) at 1981-99
746 levels. 43
- 747 8 Residual % changes in climatological annual-mean PET between 1981-99 and
748 2081-99 that remain after subtracting off the pieces attributed to ($R_n - G$),
749 T_a , RH, and $|u|$ (Figures 4-7) from the raw change (Figure 3.) 44

- 750 9 For each model grid cell, the PET-weighted annual average $\overline{f_{\Delta}}$ of 1981-99
751 climatological f_{Δ} , the fraction of the denominator of Penman-Monteith PET
752 (5) made up by the Clausius-Clapeyron slope Δ . Last panel is the multimodel
753 mean. 45
- 754 10 For each model grid cell, the PET-weighted annual average 1981-99 climato-
755 logical temperature $\overline{T_a}$, in °C. Last panel is the multimodel mean. 46
- 756 11 Our scaling estimate $\left[d\Delta / (\Delta dT) \left(1 - \overline{f_{\Delta}} \right) + \epsilon \overline{f_{aero}} \right]$ of the relative sensitivity
757 of annual-mean PET to PET-weighted warming, from (17). Units are % deg⁻¹. 47
- 758 12 PET-weighted annual average of climate warming $\overline{dT_a}$ between 1981-99 and
759 2081-99. Units are deg. 48
- 760 13 Our scaling estimate (the exponential of (17) minus 1) for the % changes in
761 climatological annual-mean PET from setting only the ambient air temper-
762 ature T_a to 2081-99 levels while leaving all other variables in (5), including
763 relative humidity RH, at 1981-99 levels. Compare to Figure 5. Last panel
764 is the estimated % change in the multimodel mean given these estimates for
765 each model. 49
- 766 14 % changes in climatological annual-mean PET from setting only the ambient
767 air temperature T_a to 2081-99 levels while leaving all other variables in (5) at
768 1981-99 levels, for the version of (5) in which $r_s \equiv 0$. Compare to Figure 5. 50

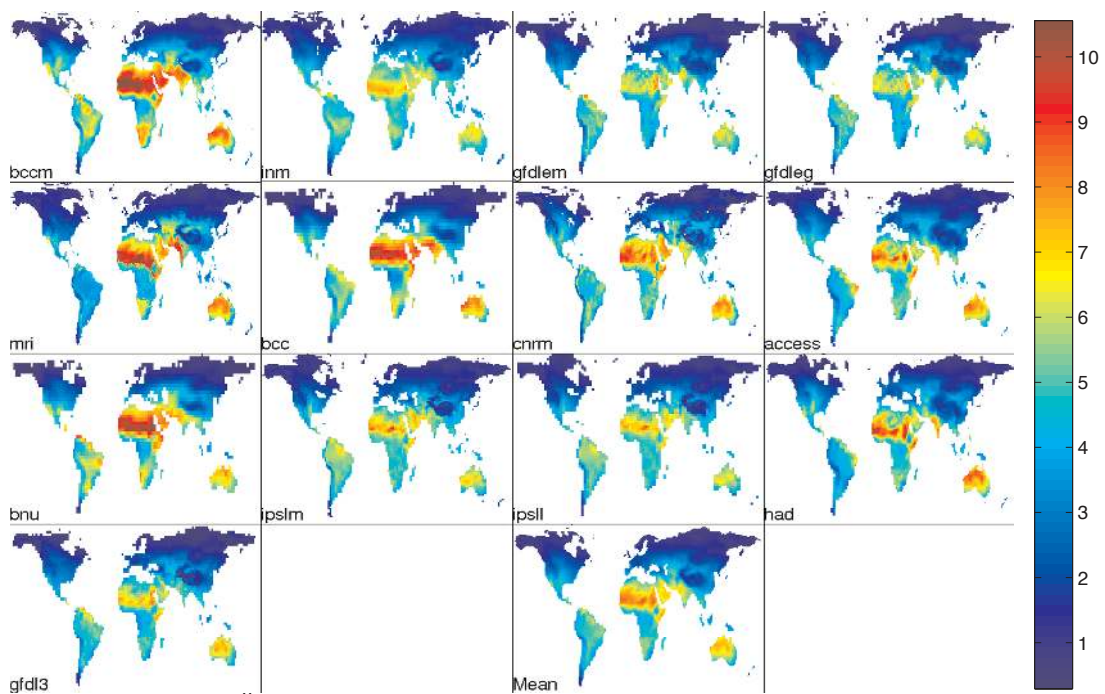


FIG. 1. 1981-99 climatological annual-mean Penman-Monteith PET (5) in mm day⁻¹ for each CMIP5 model in Table 1. Last panel is the mean over all applicable models (omitting locations where less than half of the models were analyzed.)

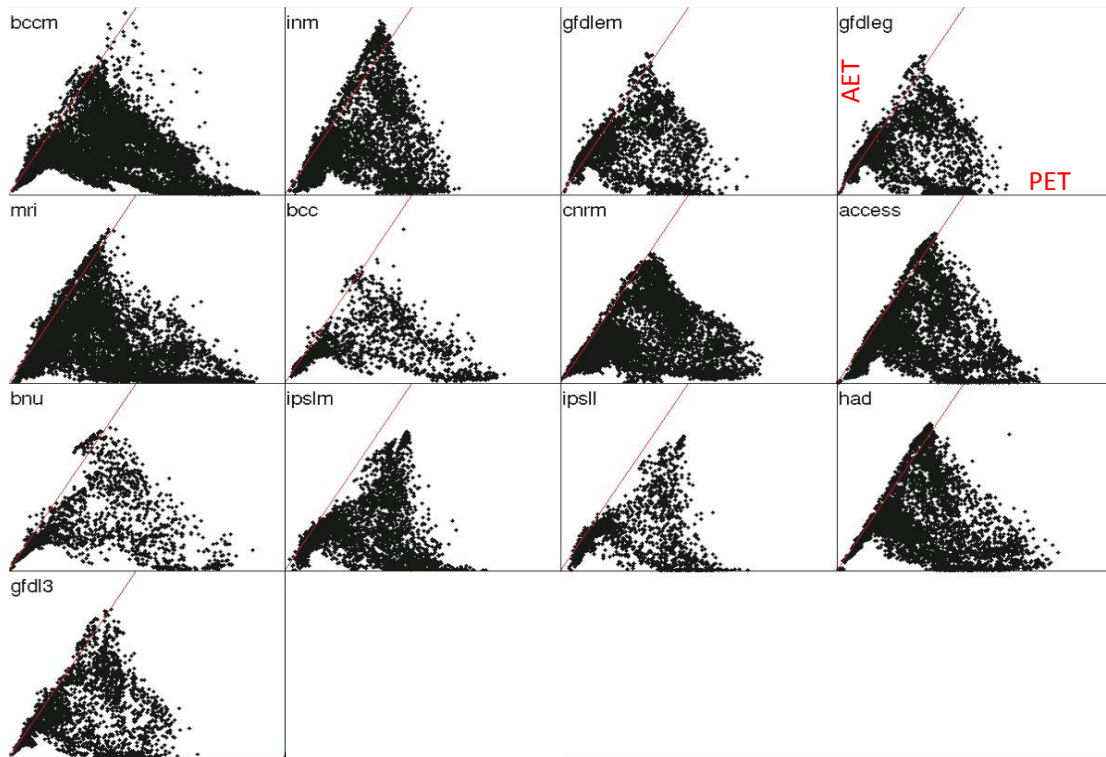


FIG. 2. 1981-99 climatological annual-mean actual ET (vertical, $0-6 \text{ mm day}^{-1}$) vs. PET (horizontal, $0-13 \text{ mm day}^{-1}$) for each model, where each dot is one grid cell. Red lines are 1:1 (actual ET = PET.)

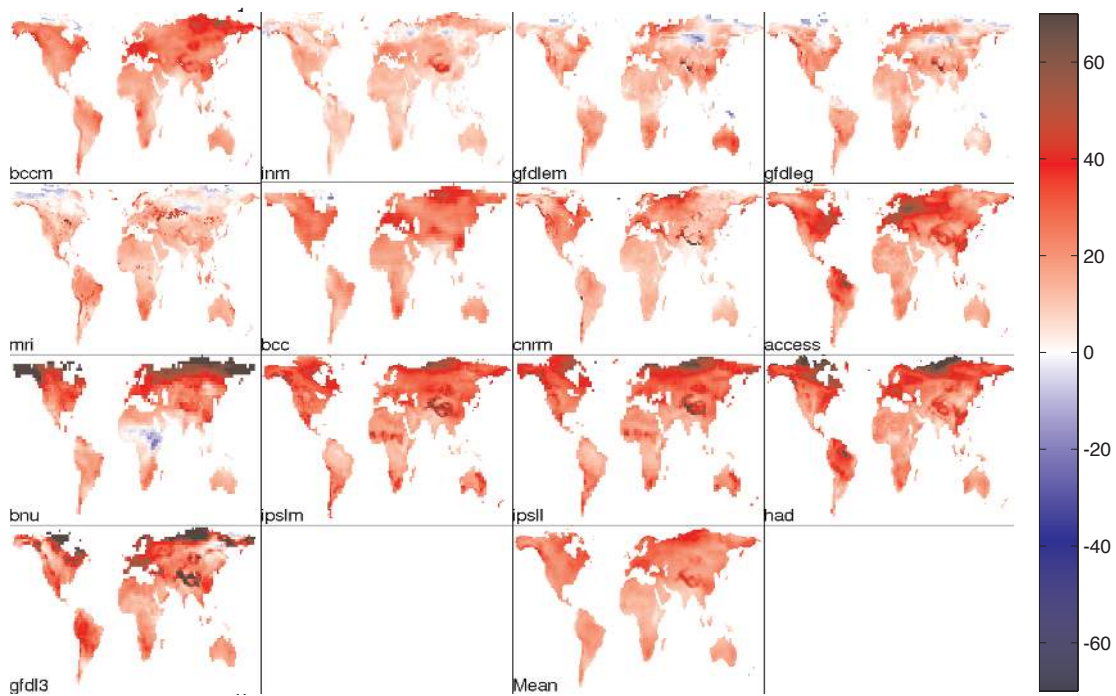


FIG. 3. % changes in climatological annual-mean PET between 1981-99 and 2081-99, for each model. (Values in a few color-saturated regions greatly exceed those on the scale.) Last panel is the % change in the multimodel mean.

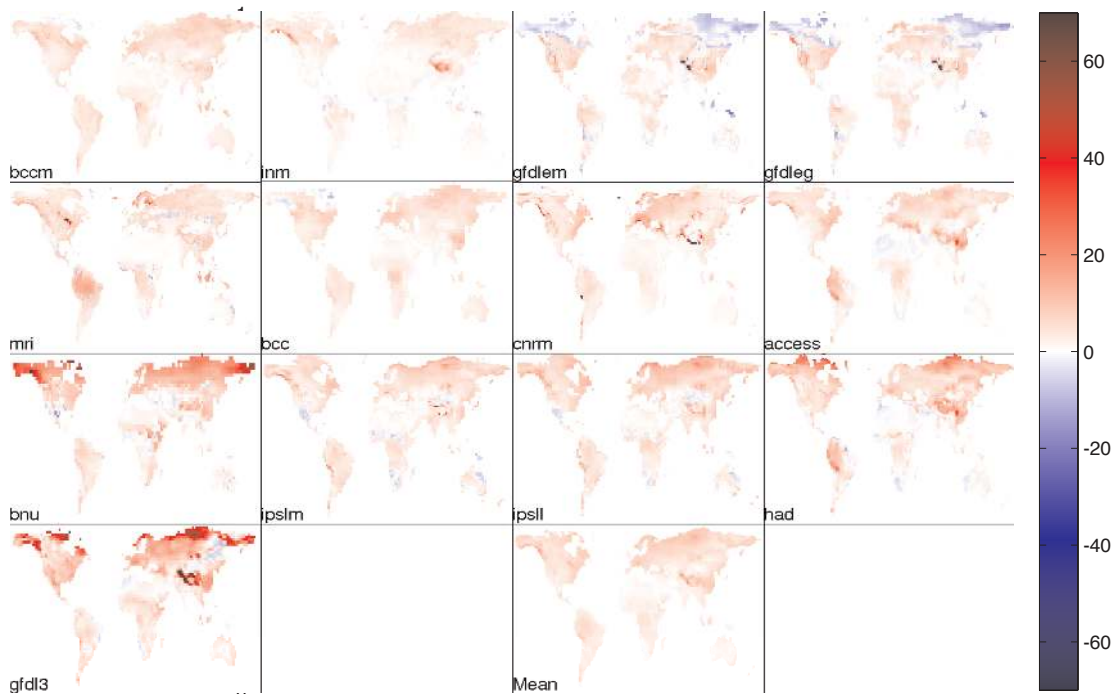


FIG. 4. % changes in climatological annual-mean PET from setting only the surface radiative energy supply ($R_n - G$) to 2081-99 levels while leaving all other variables in (5) at 1981-99 levels.

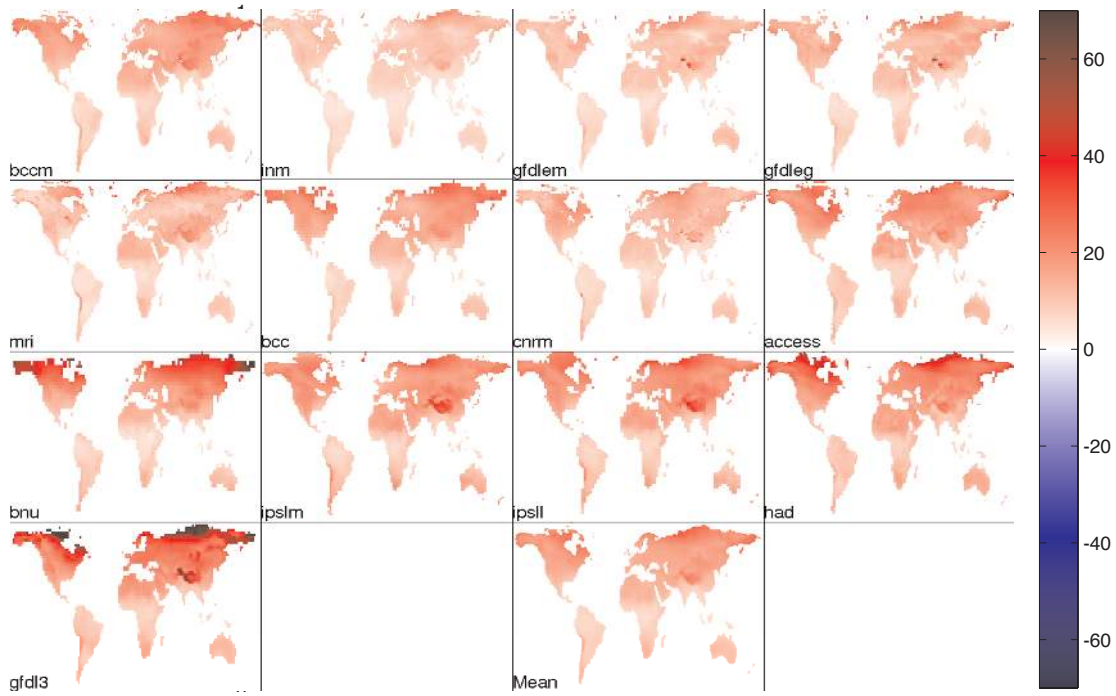


FIG. 5. % changes in climatological annual-mean PET from setting only the ambient air temperature T_a (and thus the saturation vapor pressure e^* and its derivative Δ) to 2081-99 levels while leaving all other variables in (5), including relative humidity RH, at 1981-99 levels.

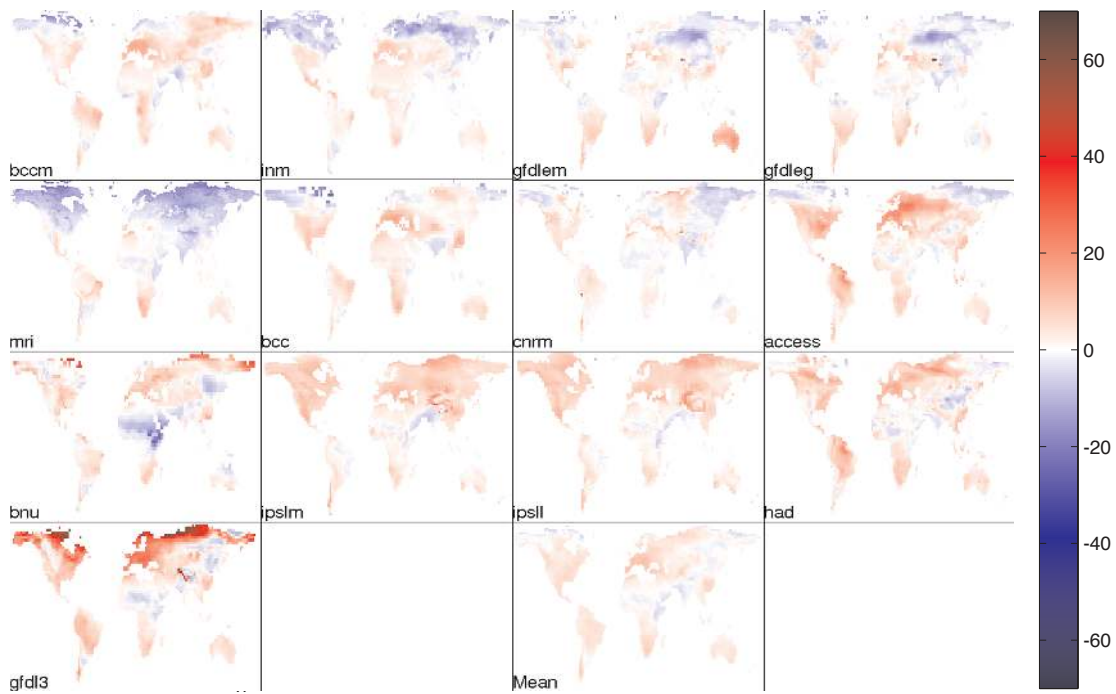


FIG. 6. % changes in climatological annual-mean PET from setting only the relative humidity RH to 2081-99 levels while leaving all other variables in (5) at 1981-99 levels.

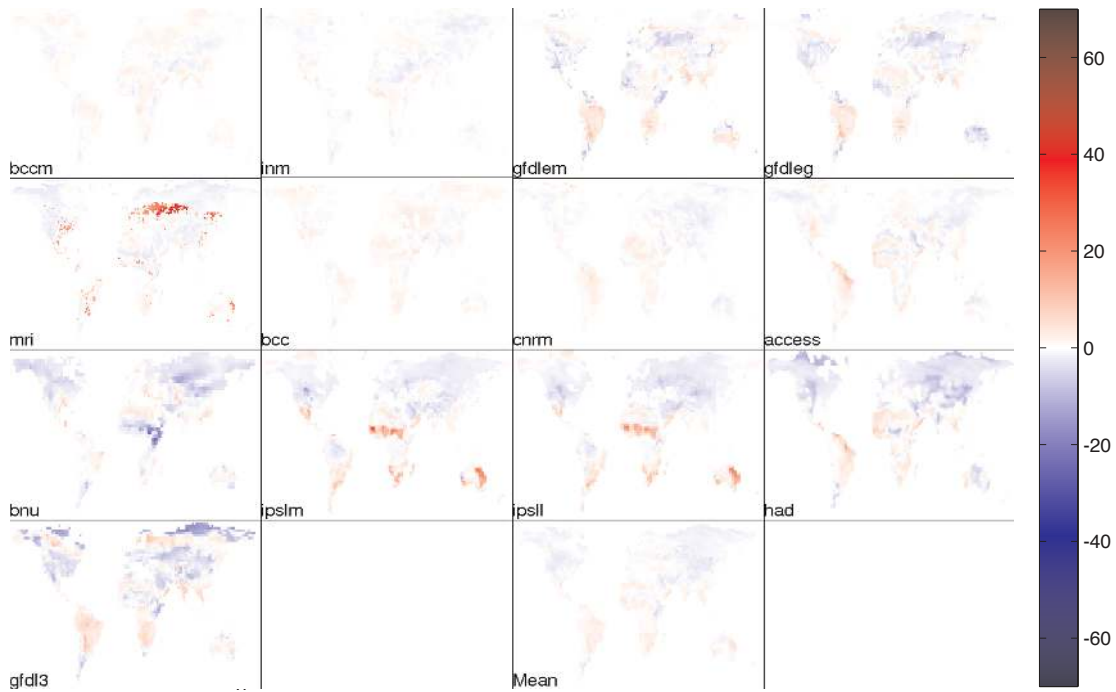


FIG. 7. % changes in climatological annual-mean PET from setting only the windspeed $|u|$ to 2081-99 levels while leaving all other variables in (5) at 1981-99 levels.

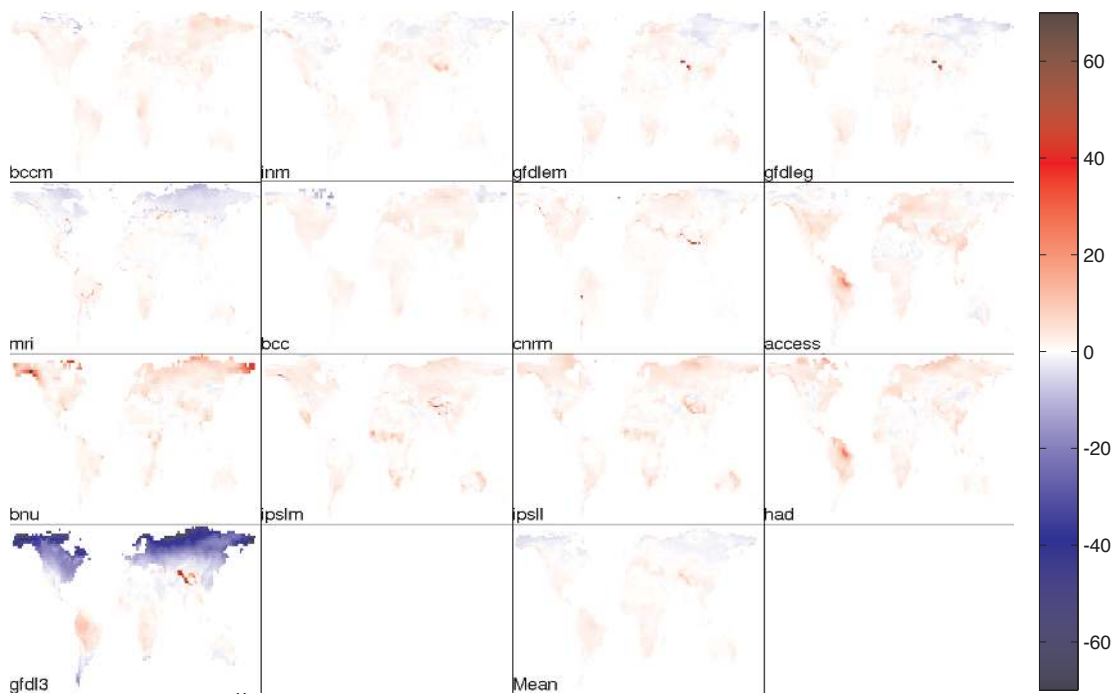


FIG. 8. Residual % changes in climatological annual-mean PET between 1981-99 and 2081-99 that remain after subtracting off the pieces attributed to $(R_n - G)$, T_a , RH, and $|u|$ (Figures 4-7) from the raw change (Figure 3.)

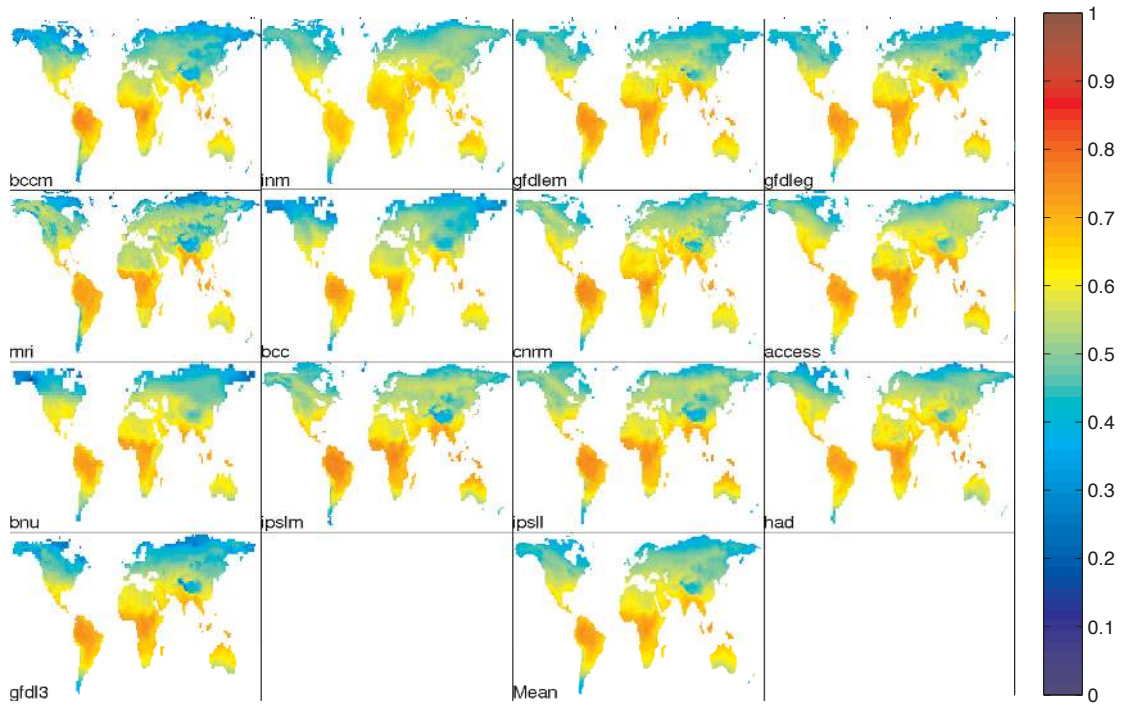


FIG. 9. For each model grid cell, the PET-weighted annual average $\overline{f_{\Delta}}$ of 1981-99 climatological f_{Δ} , the fraction of the denominator of Penman-Monteith PET (5) made up by the Clausius-Clapeyron slope Δ . Last panel is the multimodel mean.

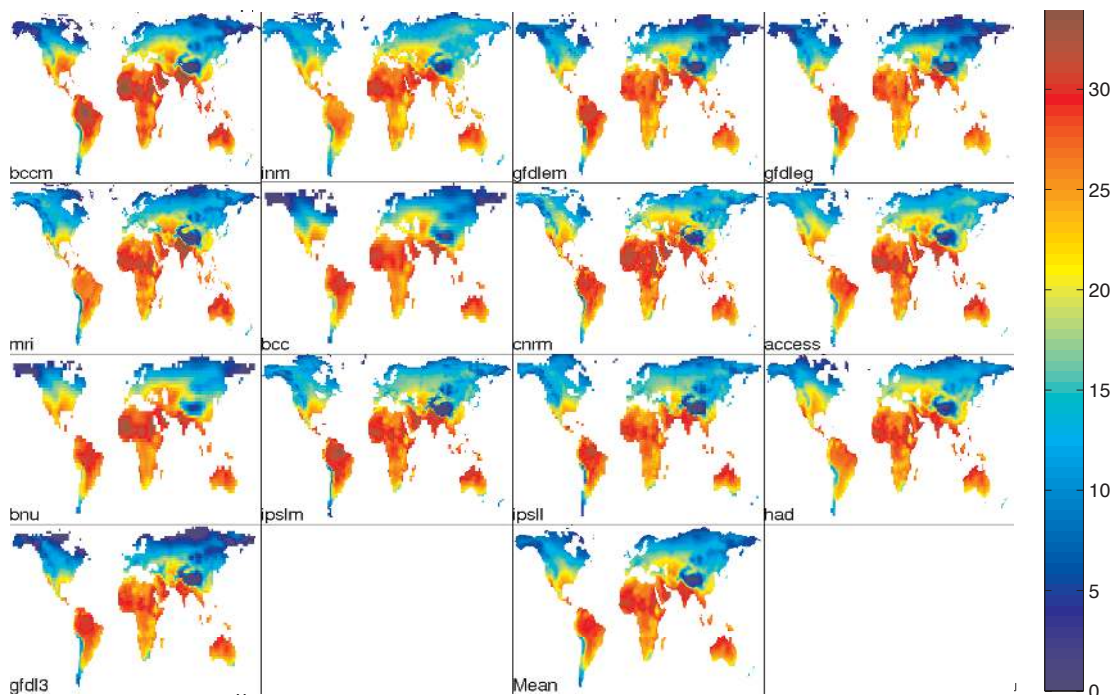


FIG. 10. For each model grid cell, the PET-weighted annual average 1981-99 climatological temperature \overline{T}_a , in $^{\circ}\text{C}$. Last panel is the multimodel mean.

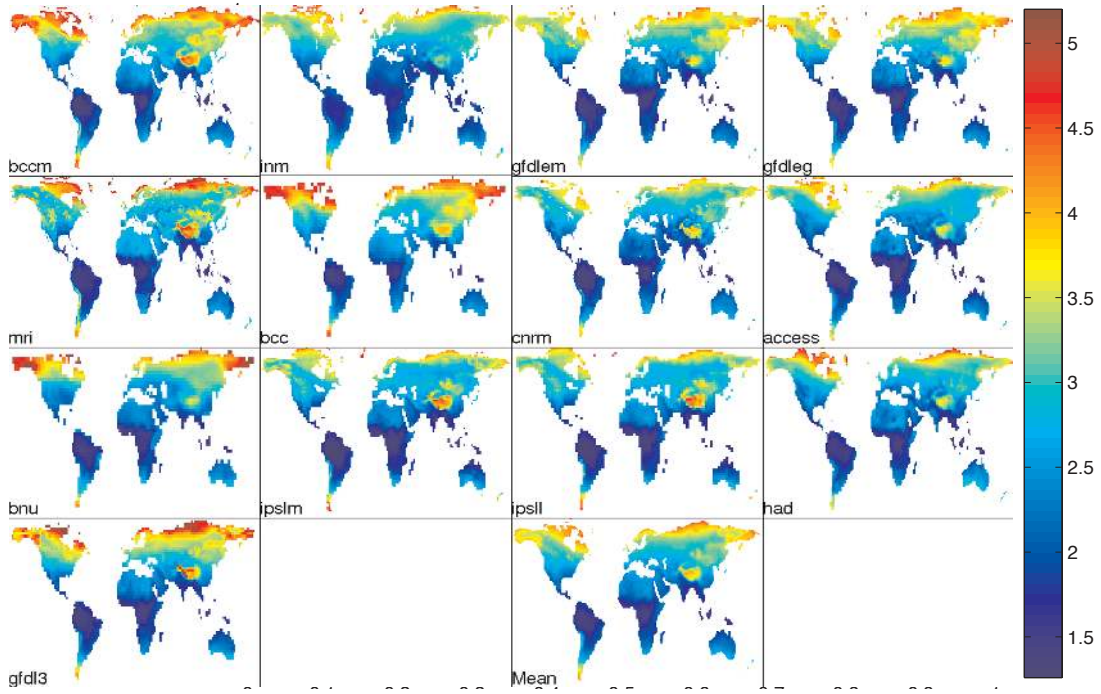


FIG. 11. Our scaling estimate $\left[d\Delta / (\Delta dT) \left(1 - \overline{f_{\Delta}} \right) + \overline{\epsilon f_{aero}} \right]$ of the relative sensitivity of annual-mean PET to PET-weighted warming, from (17). Units are $\% \text{ deg}^{-1}$.

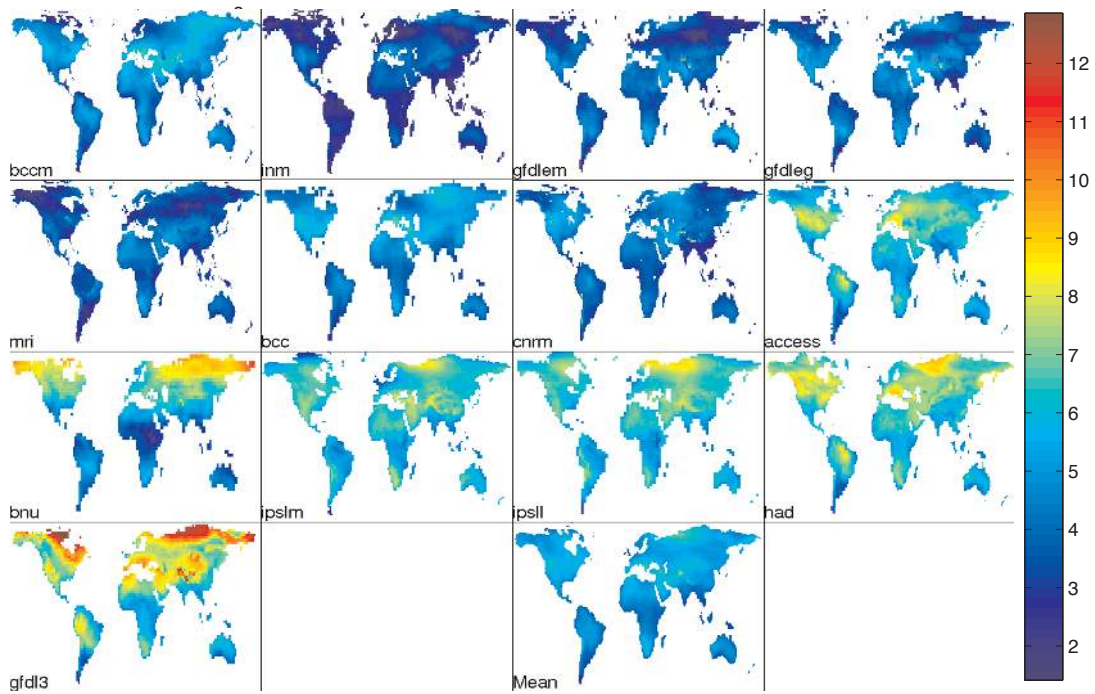


FIG. 12. PET-weighted annual average of climate warming $\overline{\overline{dT_a}}$ between 1981-99 and 2081-99. Units are deg.

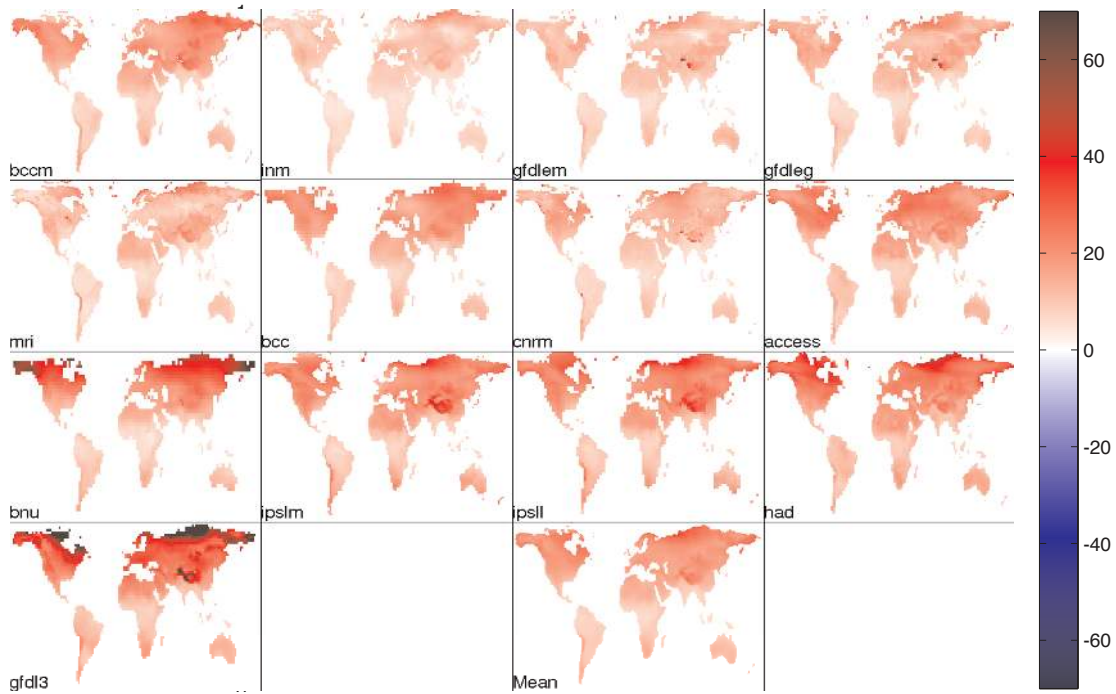


FIG. 13. Our scaling estimate (the exponential of (17) minus 1) for the % changes in climatological annual-mean PET from setting only the ambient air temperature T_a to 2081-99 levels while leaving all other variables in (5), including relative humidity RH, at 1981-99 levels. Compare to Figure 5. Last panel is the estimated % change in the multimodel mean given these estimates for each model.

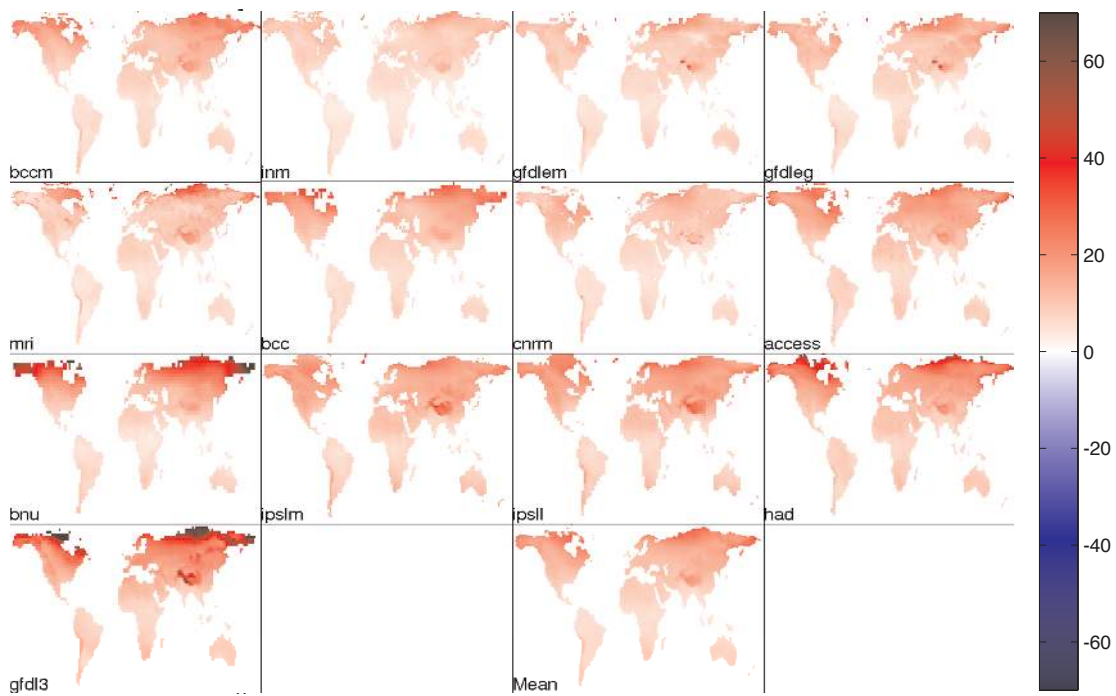


FIG. 14. % changes in climatological annual-mean PET from setting only the ambient air temperature T_a to 2081-99 levels while leaving all other variables in (5) at 1981-99 levels, for the version of (5) in which $r_s \equiv 0$. Compare to Figure 5.